IEEE Access
Multidisciplinary ⋮ Rapid Review ⋮ Open Access Journal

Received 15 July 2022, accepted 2 August 2022, date of publication 26 August 2022, date of current version 31 August 2022.

Digital Object Identifier 10.1109/ACCESS.2022.3197790

RESEARCH ARTICLE

A New 5-D Multistable Hyperchaotic System With Three Positive Lyapunov Exponents: Bifurcation Analysis, Circuit Design, FPGA Realization and Image Encryption

KHALED BENKOUIDER[1], SUNDARAPANDIAN VAIDYANATHAN[2], ACENG SAMBAS[3,8], ESTEBAN TLELO-CUAUTLE[4], AHMED A. ABD EL-LATIF[5,6], (Senior Member, IEEE), BASSEM ABD-EL-ATTY[7], CIRO FABIAN BERMUDEZ-MARQUEZ[4], IBRAHIM MOHAMMED SULAIMAN[8], ALIYU MUHAMMED AWWAL[9,10,11], AND POOM KUMAM[9,12], (Member, IEEE)

[1]Non Destructive Testing Laboratory, Automatic Department, University of Jijel, Jijel 18000, Algeria
[2]School of Electrical and Communication Engineering, Vel Tech University, Avadi, Chennai, Tamil Nadu 600062, India
[3]Department of Mechanical Engineering, Universitas Muhammadiyah Tasikmalaya, Tasikmalaya, Jawa Barat 46196, Indonesia
[4]Department of Electronics, Instituto Nacional de Astrofísica, Óptica y Electrónica (INAOE), Puebla 72840, Mexico
[5]EIAS Data Science Laboratory, College of Computer and Information Sciences, Prince Sultan University, Riyadh 11586, Saudi Arabia
[6]Department of Mathematics and Computer Science, Faculty of Science, Menoufia University, Menoufia 32511, Egypt
[7]Department of Computer Science, Faculty of Computers and Information, Luxor University, Luxor 85957, Egypt
[8]School of Quantitative Sciences, Institute of Strategic Industrial Decision Modelling (ISIDM), Universiti Utara Malaysia, Sintok, Kedah 06010, Malaysia
[9]KMUTT Fixed Point Research Laboratory, Room SCL 802 Fixed Point Laboratory, Science Laboratory Building, Center of Excellence in Theoretical and Computational Science (TaCS-CoE), Departments of Mathematics, Faculty of Science, King Mongkut's University of Technology Thonburi (KMUTT), Thung Khru, Bangkok 10140, Thailand
[10]Department of Mathematics, Faculty of Science, Gombe State University, Gombe 760214, Nigeria
[11]GSU-Mathematics for Innovative Research (GSU-MIR) Group, Gombe State University, Gombe 760214, Nigeria
[12]Department of Medical Research, China Medical University Hospital, China Medical University, Taichung 40402, Taiwan

Corresponding author: Poom Kumam (poom.kum@kmutt.ac.th)

The authors acknowledge the financial support provided by the Center of Excellence in Theoretical and Computational Science (TaCS-CoE), KMUTT. Moreover, this research project is supported by Thailand Science Research and Innovation (TSRI) Basic Research Fund: Fiscal year 2022 under project number FRB650048/0164. The authors acknowledge the financial support provided by "Mid-Career Research Grant" (N41A640089).

ABSTRACT In this work, we describe the model of a new 5-D hyperchaotic system with three positive Lyapunov exponents. Since the maximum positive Lyapunov exponent of the proposed hyperchaotic system is larger than twelve, the new hyperchaotic system is highly hyperchaotic. We also show that the new 5-D hyperchaotic system exhibits multistability with coexisting attractors. Using Multisim, we design an electronic circuit for the new 5-D hyperchaotic system. The hardware implementation of the new 5-D hyperchaotic system is done by applying two numerical methods. From the experimental results of the FPGA-based implementation, we show that the attractors observed in a Lecroy oscilloscope are in good agreement with numerical simulations. To prove the reliability of the proposed system for cybersecurity purposes, we present a new image cryptosystem using our hyperchaotic system. Experimental outcomes show the efficiency and the reliability of our cryptosystem based on the proposed hyperchaotic system.

INDEX TERMS Hyperchaos, hyperchaotic systems, bifurcations, multi-stability, attractors, Lyapunov exponents, circuit design, FPGA, numerical methods, data security, image cryptosystem.

I. INTRODUCTION

Hyperchaotic systems have several applications in engineering and science due to their high complexity [1]. Bian and Yu [2] described a new chaotic communication

The associate editor coordinating the review of this manuscript and approving it for publication was Christian Pilato.

encryption method based on a 6-D hyperchaotic Lorenz system and performed a circuit simulation to verify the security of the communication scheme. Wang *et al.* [3] designed a 6-D hyperchaotic system and applied it to complete the signal encryption and decryption circuit design of a secure communication scheme. Peng *et al.* [4] proposed a new 5-D hyperchaotic system for secure communication based on Micro Controller Unit (MCU). Xiu *et al.* [5] presented a memristive cellular neural network (CNN) hyperchaotic system and described its hardware circuit design. Li *et al.* [6] presented a new 5-D memristive hyperchaotic system based on hyperchaotic Lü system and described its extreme multistability. Alibraheemi *et al.* [7] described the design and simulation of a 4-D hyperchaotic communication system based on the Lorenz chaotic attractor.

In this work, we describe the model of a new 5-D hyperchaotic system with three equilibrium points and deduce that the new hyperchaotic system has three positive Lyapunov exponents (LE). We show that the maximum positive Lyapunov exponent of the proposed hyperchaotic system is larger than twelve. Thus, we observe that the new hyperchaotic system is highly hyperchaotic.

We present a detailed dynamic analysis for the new 5-D hyperchaotic system with bifurcation diagrams and Lyapunov exponents. Bifurcation analysis is useful for understanding the dynamic behavior of hyperchaotic systems with respect to changes in values of the system parameters [8], [9], [10]. We also note that the new hyperchaotic system exhibits multistability with coexisting attractors.

The application of electronic circuits in the hyperchaotic system has been widely explored by researchers such as secure communication system, high frequency generator, robotic, structure optimization of antenna arrays, satellite communications, autonomous unmanned aerial vehicles and sound encryption [11], [12], [13]. Using Multisim, we design an electronic circuit for the implementation of the new 5-D hyperchaotic system and present the circuit simulation results. Circuit design for chaotic and hyperchaotic systems has important applications in engineering [11], [12], [13], [14].

Autonomous and nonautonomous chaotic systems have been implemented with different analog and digital electronic devices. For instance, the recent paper in [15] shows the electronic implementation of an autonomous chaotic and hyperchaotic system made of a Colpitts-Josephson junction like circuit and three physical energy storage tanks, namely CLC. The circuit is simulated using the simulation program with integrated circuit emphasis (SPICE), and also, the authors implement the chaotic system using Arduino UNO board that is based on a microcontroller. In a similar way, the authors in [16], introduce a new 4D hyperchaotic system showing its analog and digital Implementation. The analog implementation is performed using amplifiers, and the digital implementation using a Digital Signal Processor (DSP), which showed good agreement with simulation results. The design of chaotic systems can also be performed using integrated circuit technology [17], however, due to the design challenges when using nanometer technologies, authors prefer reconfigurable hardware. For instance, one decade ago the authors in [18] demonstrated the usefulness of the field-programmable analog array (FPAA) to design chaotic systems, emphasizing that this device provides flexible design possibilities such as reducing the complexity of design, real-time modification, software control and adjustment within the system. Other works that use FPAAs to implement chaotic systems can be found in [19], [20], [21], [22].

Although amplifiers, FPAAs and microcontrollers have demonstrated their usefulness in implementing chaotic systems, the field-programmable gate array (FPGA) device is more appropriate for fast prototyping and verification of chaotic attractors. The FPGA is a programmable device that can be configured to implement the functionality comparable to custom hardware without requiring additional fabrication steps, printed circuit board fabrication, etc. In addition, it facilitates parallel computing because each different computing task can be assigned to a dedicated group of logic blocks. In Sect. VII we show details on the FPGA design of this new 5-D chaotic system with three positive Lyapunov exponents.

Data security acts a vital role in present days, in which digital images represent the familiar model of representing data [23]. The information existing in digital images can be protected via applying one of image encryption and/or data hiding algorithms [24]. Chaotic maps are considered the backbone of designing modern image encryption techniques [12], [25], [26]. In this paper, we presented a new color image cryptosystem based on the presented 5-D hyperchaotic map. Experimental outcomes demonstrate the efficiency and the reliability of our cryptosystem, accordingly, our hyperchaotic system can be dependable in various security applications.

II. A NEW 5-D HYPERCHAOTIC SYSTEM

A. MATHEMATICAL MODEL OF THE NEW SYSTEM

In this paper, we propose a new 5-D hyperchaotic system modelled by the dynamics

$$\begin{cases} \dot{z}_1 = a(z_2 - z_1) + z_2 z_3 + z_4 \\ \dot{z}_2 = z_1(b - z_3) + c z_4 \\ \dot{z}_3 = z_1^2 + z_1 z_2 - d z_3 \\ \dot{z}_4 = -z_2 + z_5 \\ \dot{z}_5 = -z_4 \end{cases} \tag{1}$$

where z_1, z_2, z_3, z_4, z_5 are the states and a, b, c, d are parameters.

In this work, we establish that the system (1) is *hyperchaotic* with three positive Lyapunov exponents if we take the initial state as $Z(0) = (1, 1, 1, 1, 1)$ and parameters as

$$a = 40, \quad b = 90, \quad c = 16, \quad d = 15 \tag{2}$$

The system (1) stays invariant under the change of coordinates

$$(z_1, z_2, z_3, z_4, z_5) \mapsto (-z_1, -z_2, z_3, -z_4, -z_5) \tag{3}$$

for all values of the system parameters. This shows that the system (1) has rotational symmetry about the z_3-axis.

B. DYNAMIC PROPERTIES OF THE NEW SYSTEM

Using Matlab, we calculated the Lyapunov exponents of the 5-D system (1) for the initial state $Z(0) = (1, 1, 1, 1, 1)$, $(a, b, c, d) = (40, 90, 16, 15)$ and $T = 1E5$ seconds as

$$\begin{cases} LE_1 &= 12.659 \\ LE_2 &= 0.055 \\ LE_3 &= 0.024 \\ LE_4 &= 0 \\ LE_5 &= -67.7001 \end{cases} \tag{4}$$

The Kaplan-Yorke dimension of the 5-D system (1) is calculated as follows:

$$D_{KY} = 4 + \frac{LE_1 + LE_2 + LE_3 + LE_4}{|LE_5|} = 4.189 \tag{5}$$

From (4), we deduce that the 5-D system (1) is a dissipative hyperchaotic system with three positive Lyapunov exponents. Since the value of maximum Lyapunov exponent (MLE) in Eq. (4) is large, we conclude that the 5-D system is highly hyperchaotic and this property is very useful for applications of the hyperchaotic system in cryptosystems and secure communications.

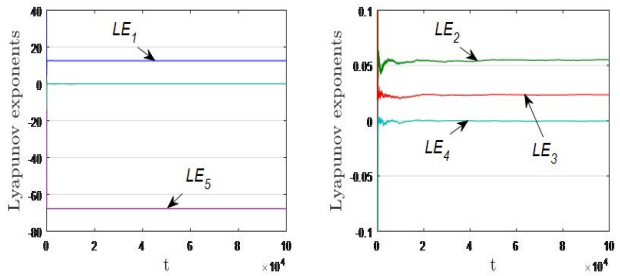

(a) (b)

FIGURE 1. MATLAB plot showing the calculation of Lyapunov exponents of the new 5-D hyperchaotic system (1) for $Z(0) = (1, 1, 1, 1, 1)$, $(a, b, c, d) = (40, 90, 16, 15)$ and $T = 1E5s$.

Figure 1 depicts the MATLAB plot showing the calculation of Lyapunov exponents of the new 5-D hyperchaotic system (1) for $Z(0) = (1, 1, 1, 1, 1)$, $(a, b, c, d) = (40, 90, 16, 15)$ and $T = 1E5$ sec.

The equilibrium points of the 5-D system (1) are found by solving the following equations.

$$3a(z_2 - z_1) + z_2 z_3 + z_4 = 0 \tag{6a}$$

$$z_1(b - z_3) + cz_4 = 0 \tag{6b}$$

$$z_1^2 + z_1 z_2 - dz_3 = 0 \tag{6c}$$

$$-z_2 + z_5 = 0 \tag{6d}$$

$$-z_4 = 0 \tag{6e}$$

Clearly, $E_0 = \mathbf{0} \in \mathbf{R}^5$ is an equilibrium point.

A simple calculation shows that there are two more equilibrium points given by

$$E_{1,2} = \begin{bmatrix} \pm\lambda\sqrt{\frac{bd}{\lambda^2+\lambda}} \\ \pm\sqrt{\frac{bd}{\lambda^2+\lambda}} \\ b \\ 0 \\ \pm\lambda\sqrt{\frac{bd}{\lambda^2+\lambda}} \end{bmatrix} \tag{7}$$

where

$$\lambda = \frac{a+b}{a} \tag{8}$$

Suppose we take the parameters as in the hyperchaotic case (2), *i.e.* $a = 40$, $b = 90$, $c = 16$ and $d = 15$.

For this case, $\lambda = \frac{a+b}{a} = 3.25$.

Also, the three equilibrium points of the system (1) are obtained as

$$\begin{cases} E_0 &= (0, 0, 0, 0, 0) \\ E_1 &= (32.1302, 9.8862, 90, 0, 9.8862) \\ E_2 &= (-32.1302, -9.8862, 90, 0, -9.8862) \end{cases} \tag{9}$$

Figure 2 depicts the 2-D MATLAB plots of the 5-D hyperchaotic system (1) with three positive Lyapunov exponents for $Z(0) = (1, 1, 1, 1, 1)$ and $(a, b, c, d) = (40, 90, 16, 15)$.

C. COMPARISON BETWEEN THE NEW 5-D HYPERCHAOTIC SYSTEM AND TEN RECENTLY REPORTED 5-D HYPERCHAOTIC SYSTEMS

From the viewpoint of Lyapunov exponents, an n-dimensional hyperchaotic system is more complex when it has more number of positive Lyapunov exponents ($n - 2$ positive Lyapunov exponents), which indicates that the dynamic of the system can expand in several directions in the phase space. In addition, a large positive Lyapunov exponent means that the system dynamic has a very fast exponential expansion in the phase space, providing stronger hyperchaotic behavior [27]. Moreover, the Kaplan-York dimension measures the complexity of the attractor. A high value of the Kaplan-Yorke dimension corresponds to a highly complex attractor. Based on the above discussions, a strong 5-D hyperchaotic system must have the following three properties:

(i) Three positive Lyapunov exponents to ensure that the dynamics of the system expand in three different directions of phase space.

(ii) A large positive Lyapunov exponent to ensure a fast exponential expansion in phase space.

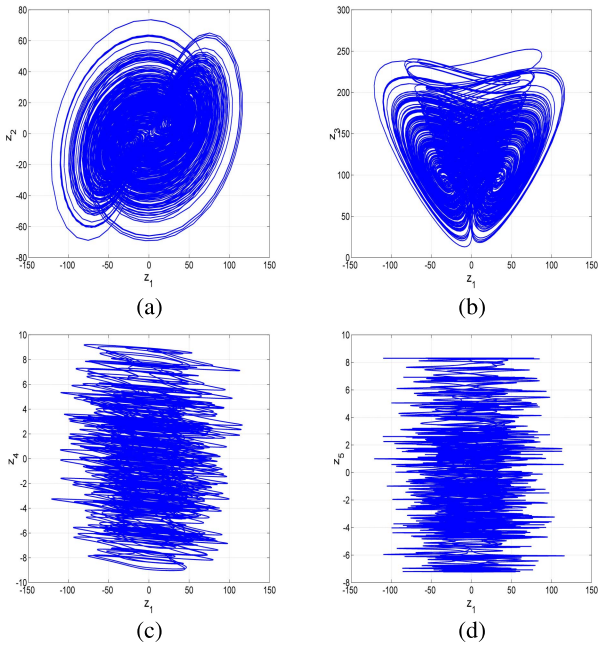

FIGURE 2. 2-D signal plots of the 5-D hyperchaotic system (1) with three positive Lyapunov exponents for $Z(0) = (1, 1, 1, 1, 1)$ and $(a, b, c, d) = (40, 90, 16, 15)$: (a) (z_1, z_2) plane, (b) (z_1, z_3) plane, (c) (z_1, z_4) plane and (d) (z_1, z_5) plane.

(iii) A high value of Kaplan-York dimension to ensure a high complexity of the attractor.

Table 1 shows the Lyapunov exponents and the Kaplan-Yorke dimension of the new system (1) and those of ten recently reported 5-D hyperchaotic systems. It can be seen that the new system (1) has three positive Lyapunov exponents, contrary to many other reported 5-D systems that have two positive Lyapunov exponents. Also, system (1) has the largest first Lyapunov exponent, which means that its trajectories expand more quickly than those of other reported 5-D systems. Finally, we can see that the new system (1) has a much larger Kaplan-Yorke dimension than that of the most recently reported 5-D hyperchaotic systems. As a result, the new 5-D hyperchaotic system is much stronger than many reported 5-D hyperchaotic systems. It is a big addition to the hyperchaotic systems family. Its properties make it very desirable to use in chaos-based applications.

III. BIFURCATION ANALYSIS OF THE NEW 5-D HYPERCHAOTIC SYSTEM

In this section, the dynamical properties of the 5-D hyperchaotic system (1) are investigated using Lyapunov exponents spectrums, bifurcation diagrams and phases plots. Influence of the system parameters on the behavior of the new highly-complex hyperchaotic system (1) will be presented when $Z(0) = (1, 1, 1, 1, 1)$.

A. DYNAMICAL BEHAVIOR EVOLUTION WHEN a CHANGES

Dynamical properties of the 5-D system (1) are presented here when the value of parameter a increases in the region $[10, 40]$, while the other parameters are fixed as $b = 90$, $c = 16$ and $d = 12$.

Simulation results shows that system (1) can present different behaviors for different values of parameter a.

Bifurcation diagram presented in Figure 3 (a) and Lyapunov exponents spectrum shown in Figure 3 (b) demonstrate that, based on the values of the control parameter a, the 5-D system (1) can exhibit periodic behavior, chaotic behavior with small value of maximal Lyapunov exponent (MLE), hyperchaotic behavior with two positive Lyapunov exponents and high value of MLE or hyperchaotic behavior with three positive Lyapunov exponents and a very high value of MLE.

Define $A = [0, 18.5] \cup [19.2, 20]$.

When $a \in A$, the MLE of the new 5-D system (1) is zero, implying that system (1) displays periodic behavior with no complexity. We chose the control parameter $a = 12$. Then, the periodic attractor is plotted in (z_1, z_2) plane in Figure 4 (a). The corresponding Lyapunov exponents are:

$$\begin{cases} LE_1 &= 0 \\ LE_2 &= -0.117 \\ LE_3 &= -0.118 \\ LE_4 &= -11.874 \\ LE_5 &= -11.898 \end{cases} \tag{10}$$

Define $B = [18.5, 19.2] \cup [20, 20.4]$.

When $a \in B$, the system dynamics (1) changes from periodic to chaotic via the famous period-doubling route to chaos as shown in Figure 3 (c). The MLE is positive and the Kaplan-Yorke dimension has a fractional value of 2.044, which demonstrates that the system (1) generates complex chaotic behavior for the mentioned region of control parameter. When $a = 19$, the chaotic attractor is plotted in (z_1, z_2) plane in Figure 4 (b). The corresponding Lyapunov exponents are:

$$\begin{cases} LE_1 &= 0.011 \\ LE_2 &= 0 \\ LE_3 &= -0.252 \\ LE_4 &= -3.447 \\ LE_5 &= -27.307 \end{cases} \tag{11}$$

When $a \in [20.4, 32]$, the 5-D system dynamics (1) changes from chaotic to hyperchaotic with two positive Lyapunov exponents and a high value of MLE. Thus, in this region of control parameters, the system (1) displays a very complex hyperchaotic behavior characterized with the following fractional value of Kaplan-Yorke dimension $D_{KY} = 4.219$. When $a = 25$, the chaotic attractor is plotted in (z_1, z_2) plane

TABLE 1. A comparison of Lyapunov exponents and Kaplan-Yorke dimension of ten recently reported 5-D hyperchaotic systems and the new 5-D hyperchaotic system.

System	LE_1	LE_2	LE_3	LE_4	LE_5	D_{KY}
System 1 [28]	6.053	0.028	0	−4.747	−46.214	4.029
System 2 [29]	0.287	0.019	0	−0.612	−1.698	3.500
System 3 [30]	1.300	0.011	0	−1.111	−2.300	4.087
System 4 [31]	0.371	0.240	0	−0.169	−15.105	4.029
System 5 [32]	0.178	0.110	0	−5.185	−28.108	3.055
System 6 [33]	0.645	0.099	0	−12.682	−19.688	3.023
System 7 [34]	0.207	0.013	0.005	0	−2.226	4.101
System 8 [35]	0.990	0.328	0.295	0	−47.633	4.034
System 9 [36]	0.171	0.091	0.011	0	−2.324	4.117
System 10 [37]	0.419	0.243	0.015	0	−13.041	4.052
New system (1)	**12.659**	**0.055**	**0.024**	**0**	**−67.701**	**4.189**

in Figure 4 (c). The corresponding Lyapunov exponents are:

$$\begin{cases} LE_1 &= 10.366 \\ LE_2 &= 0.039 \\ LE_3 &= 0 \\ LE_4 &= -0.020 \\ LE_5 &= -47.382 \end{cases} \tag{12}$$

When $a \in [32, 40]$, the 5-D system dynamics (1) displays hyperchaotic behavior with three positive Lyapunov exponents and a very high value of MLE (about 12) providing extreme complexity of the dynamics.

When $a = 39.8$, the hyperchaotic attractor of the new 5-D system is plotted in (z_1, z_2) plane in Figure 4 (d) and characterized with the following fractional value of Kaplan-Yorke dimension $D_{KY} = 4.178$. The corresponding Lyapunov exponents are:

$$\begin{cases} LE_1 &= 11.862 \\ LE_2 &= 0.041 \\ LE_3 &= 0.033 \\ LE_4 &= 0 \\ LE_5 &= -63.706 \end{cases} \tag{13}$$

Behaviors, Lyapunov exponents values, Kaplan-Yorke dimensions and attractors of the new 5-D system (1) for different values of parameter a are summarized in Table 2.

B. DYNAMICAL BEHAVIOR EVOLUTION WHEN b CHANGES

Dynamical properties of the 5-D system (1) are presented here when the value of parameter b increases in the region [0, 90], while the other parameters are fixed as $a = 40$, $c = 16$ and $d = 12$.

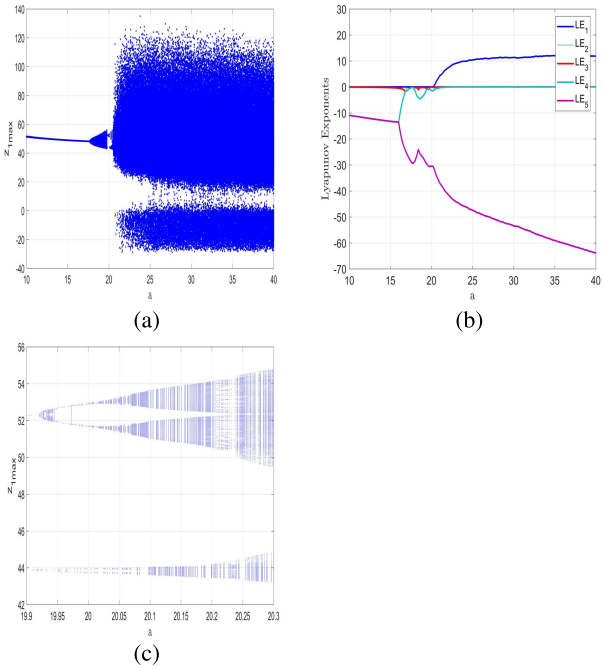

FIGURE 3. Bifurcation diagram (a) and Lyapunov exponents spectrum (b) of the new 5-D hyperchaotic system (1) when $a \in [10, 40]$, $b = 90$, $c = 16$, $d = 12$ and (c) period doubling to chaos when $a \in [19, 9, 20.3]$, $b = 90$, $c = 16$, $d = 12$.

Simulation results shows that system (1) can present different behaviors for different values of parameter b.

Bifurcation diagram presented in Figure 5 (a) and Lyapunov exponents spectrum shown in Figure 5 (b) demonstrate that, based on the values of the control parameter b, the 5-D system (1) can exhibit periodic behavior, hyperchaotic

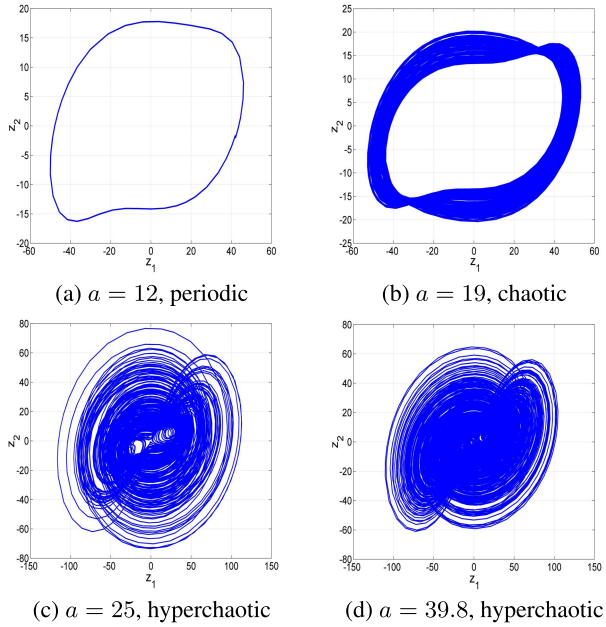

(a) $a = 12$, periodic (b) $a = 19$, chaotic

(c) $a = 25$, hyperchaotic (d) $a = 39.8$, hyperchaotic

FIGURE 4. 2-D plots of the new 5-D hyperchaotic system (1) in the (z_1, z_2) -plane for $b = 90$, $c = 16$, $d = 12$ and different values of a.

behavior with two positive Lyapunov exponents, hyperchaotic behavior with three positive Lyapunov exponents or converges to equilibrium point.

When $b \in [0, 9]$, from Figure 5 (b), we can see that the MLE of the new 5-D system is zero, implying that the system (1) displays periodic behavior, which is confirmed by bifurcation diagram in Figure 5 (a). When we choose the control parameter $b = 4$, the periodic attractor of the system (1) is plotted in (z_1, z_3)-plane in Figure 6 (a). The corresponding Lyapunov exponents are:

$$\begin{cases} LE_1 &= 0 \\ LE_2 &= -0.475 \\ LE_3 &= -0.489 \\ LE_4 &= -7.092 \\ LE_5 &= -43.936 \end{cases} \tag{14}$$

When $b \in [9, 14.5]$, from Figure 5 (b), we can see that the MLE of the new 5-D system is negative, implying that system (1) converges to equilibrium. Thus, in this region of control parameters, the system (1) displays a stable dynamics. When $b = 10$, the attractor of the new 5-D system (1) is plotted in (z_1, z_3)-plane in Figure 6 (b). The corresponding Lyapunov exponents are:

$$\begin{cases} LE_1 &= -0.198 \\ LE_2 &= -0.204 \\ LE_3 &= -1.332 \\ LE_4 &= -1.412 \\ LE_5 &= -48.511 \end{cases} \tag{15}$$

Define $C = [14.5, 19.6] \cup [23.5, 26.5]$.

When $b \in C$, the system dynamics (1) changes to hyperchaotic behavior with two positive Lyapunov exponents as shown in Figure 4 (b). Hence, in this region of control parameters, the system (1) displays a complex behavior characterized with the following fractional value of Kaplan-Yorke dimension $D_{KY} = 3.282$. When $b = 16$, the hyperchaotic attractor of the new 5-D system (1) is plotted in (z_1, z_3)-plane in Figure 6 (c). The corresponding Lyapunov exponents are:

$$\begin{cases} LE_1 &= 0.224 \\ LE_2 &= 0.127 \\ LE_3 &= 0 \\ LE_4 &= -1.246 \\ LE_5 &= -51.102 \end{cases} \tag{16}$$

Define $D = [19.6, 23.5] \cup [26.5, 90]$.

When $b \in D$, the 5-D system dynamics (1) generates hyperchaotic behavior with three positive Lyapunov exponents. When $b = 40$, the hyperchaotic attractor of the new 5-D system (1) is plotted in (z_1, z_3) plane in Figure 6 (d), and characterized with the following fractional value of Kaplan-Yorke dimension $D_{KY} = 4.080$. The corresponding Lyapunov exponents are:

$$\begin{cases} LE_1 &= 4.220 \\ LE_2 &= 0.172 \\ LE_3 &= 0.112 \\ LE_4 &= 0 \\ LE_5 &= -56.499 \end{cases} \tag{17}$$

Behaviors, Lyapunov exponents values, Kaplan-Yorke dimensions and attractors of the new 5-D system (1) for different values of parameter b are summarized in Table 2.

C. DYNAMICAL BEHAVIOR EVOLUTION WHEN c CHANGES

Dynamical properties of the 5-D system (1) are presented here when the value of parameter c increases in the region $[0, 20]$, while the other parameters are fixed as $a = 40$, $b = 90$ and $d = 12$.

Simulation results shows that system (1) can present different behaviors for different values of parameter c.

Bifurcation diagram presented in Figure 7 (a) and Lyapunov exponents spectrum shown in Figure 7 (b) demonstrate that, based on the control parameter c, the 5-D system (1) can exhibit chaotic behavior, hyperchaotic behavior with two positive Lyapunov exponents or hyperchaotic behavior with three positive Lyapunov exponents.

When $c \in [0, 1.4]$, from Figure 7 (b) we can see that there is one positive Lyapunov exponent, implying that the system (1) displays chaotic behavior, which is confirmed by bifurcation diagram in Figure 7 (a) and characterized with a fractal dimension of $D_{KY} = 4.189$. When we choose the control parameter $c = 0.3$, the chaotic attractor of the

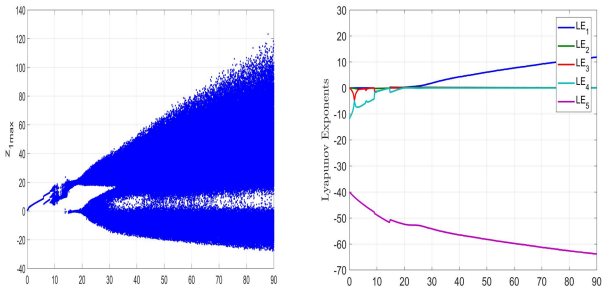

(a) (b)

FIGURE 5. Bifurcation diagram (a) and Lyapunov exponents spectrum (b) of the new 5-D hyperchaotic system (1) when $a = 40$, $c = 16$, $d = 12$ and $b \in [0, 90]$.

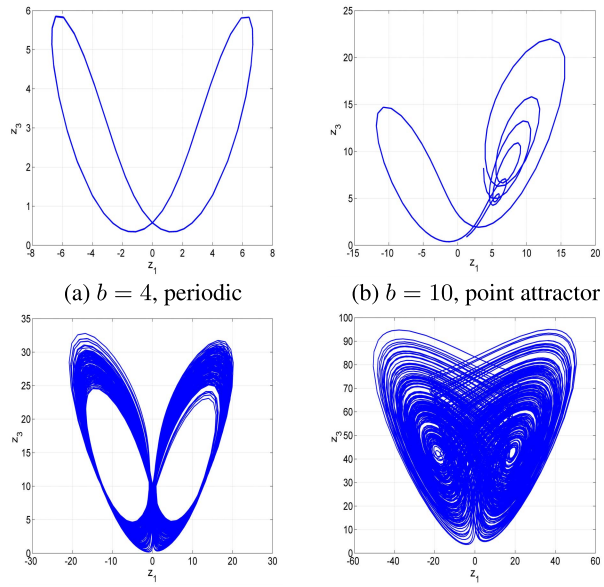

(a) $b = 4$, periodic (b) $b = 10$, point attractor

(c) $b = 16$, hyperchaotic (d) $b = 40$, hyperchaotic

FIGURE 6. 2-D plots of the new 5-D hyperchaotic system (1) in the (z_1, z_3) -plane for $a = 40$, $c = 16$, $d = 12$ and different values of b.

system (1) is plotted in (z_1, z_4) plane in Figure 8 (a). The corresponding Lyapunov exponents are:

$$\begin{cases} LE_1 & = 12.175 \\ LE_2 & = 0 \\ LE_3 & = -0.010 \\ LE_4 & = -0.017 \\ LE_5 & = -64.141 \end{cases} \tag{18}$$

When $c \in [1.4, 6]$, the system (1) dynamics change from chaos to hyperchaos with two positive Lyapunov exponents as shown in Figure 7 (b). Thus, in this region of control parameters, the system (1) dynamics expands in two different directions of phase space.

When $c = 2$, the hyperchaotic attractor of the new 5-D system (1) is plotted in (z_1, z_4)-plane in Figure 8 (b). The Kaplan-Yorke dimension is fractional with a value of $D_{KY} = 4.189$ and the corresponding Lyapunov exponents are:

$$\begin{cases} LE_1 & = 12.122 \\ LE_2 & = 0.018 \\ LE_3 & = 0 \\ LE_4 & = -0.013 \\ LE_5 & = -64.103 \end{cases} \tag{19}$$

When $c \in [6, 20]$, the system (1) exhibits hyperchaotic behaviour with three positive Lyapunov exponents. Hence, in this region of control parameters, the system (1) displays a complex behavior which expands in three different directions of phase space and characterized with the following fractional value of Kaplan-Yorke dimension $D_{KY} = 4.186$. When $c = 20$, the hyperchaotic attractor of the new 5-D system (1) is plotted in (z_1, z_4) plane in Figure 8 (c). The corresponding Lyapunov exponents are:

$$\begin{cases} LE_1 & = 11.783 \\ LE_2 & = 0.083 \\ LE_3 & = 0.031 \\ LE_4 & = 0 \\ LE_5 & = -63.867 \end{cases} \tag{20}$$

Behaviors, Lyapunov exponents values, Kaplan-Yorke dimensions and attractors of the new 5-D system (1) for different values of parameter c are summarized in Table 2.

D. DYNAMICAL BEHAVIOR EVOLUTION WHEN d CHANGES

Dynamical properties of the 5-D system (1) are presented here when the value of parameter d increases in the region $[0, 15]$, while the other parameters are fixed as $a = 40$, $b = 90$ and $c = 16$.

Simulation results show that system (1) can present different behaviors for different values of parameter d.

Bifurcation diagram presented in Figure 9 (a) and Lyapunov exponents spectrum shown in Figure 9 (b) demonstrate that, based on the control parameter d, the 5-D system (1) can exhibit chaotic behavior, hyperchaotic behavior with two positive Lyapunov exponents or hyperchaotic behavior with three positive Lyapunov exponents.

When $d \in [0, 1.1]$, the MLE of the new 5-D system is zero, implying that system (1) displays periodic behavior with no complexity. When we chose the control parameter as $d = 0.7$, then the periodic attractor of the system (1) in (z_1, z_5) plane is plotted in Figure 10 (a). The corresponding

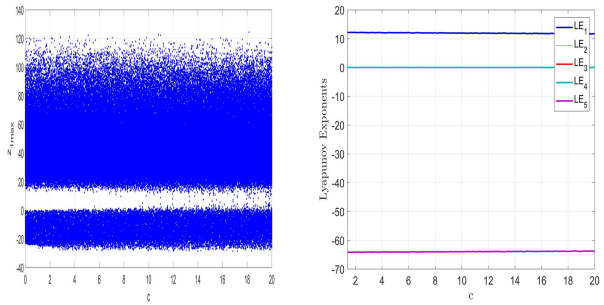

(a) (b)

FIGURE 7. Bifurcation diagram (a) and Lyapunov exponents spectrum (b) of the new 5-D hyperchaotic system (1) when $a = 40$, $b = 90$, $d = 12$ and $c \in [0, 20]$.

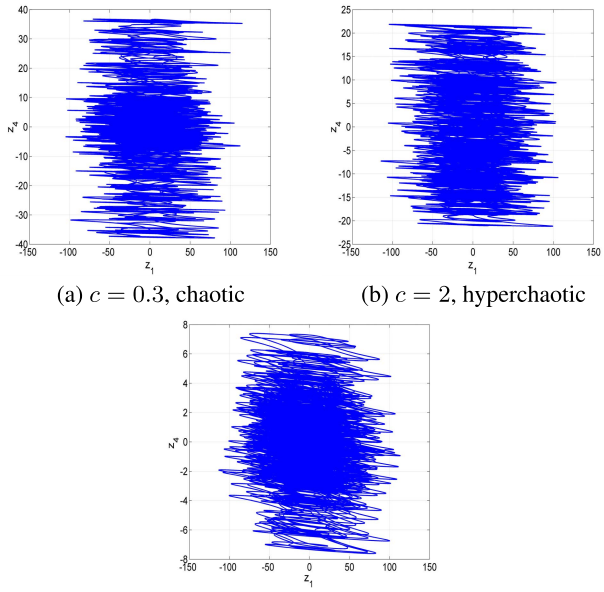

(a) $c = 0.3$, chaotic (b) $c = 2$, hyperchaotic

(c) $c = 20$, hyperchaotic

FIGURE 8. 2-D plots of the new 5-D hyperchaotic system (1) in the (z_1, z_4) -plane for $a = 40$, $b = 90$, $d = 12$ and different values of c.

Lyapunov exponents are:

$$\begin{cases} LE_1 & = 0 \\ LE_2 & = -0.580 \\ LE_3 & = -0.583 \\ LE_4 & = -1.280 \\ LE_5 & = -38.257 \end{cases} \tag{21}$$

When $d \in [1.1.7]$, system (1) dynamics change from periodic to hyperchaotic with two positive Lyapunov exponents. The MLE is over 4 and the Kaplan-Yorke dimension has a fractional value of 4.100, which demonstrates that system (1) generates complex hyperchaotic dynamics which expands in two different directions of phase space for the mentioned region of control parameter.

When $d = 4$, the hyperchaotic attractor is plotted in (z_1, z_5) plane in Figure 10 (b), which displays the hyperchaotic behavior of system (1). The corresponding Lyapunov exponents are:

$$\begin{cases} LE_1 & = 4.868 \\ LE_2 & = 0.046 \\ LE_3 & = 0 \\ LE_4 & = -0.035 \\ LE_5 & = -48.856 \end{cases} \tag{22}$$

When $d \in [7, 15]$, the system (1) displays hyperchaotic behavior with three positive Lyapunov exponents and a very high value of MLE (over 12) providing extreme complexity of the dynamics.

When $d = 14$, the hyperchaotic attractor of the new 5-D system (1) is plotted in Figure 10 (c), and characterized with the following fractional value of Kaplan-Yorke dimension $D_{KY} = 4.187$. The corresponding Lyapunov exponents are:

$$\begin{cases} LE_1 & = 12.388 \\ LE_2 & = 0.047 \\ LE_3 & = 0.017 \\ LE_4 & = 0 \\ LE_5 & = -66.420 \end{cases} \tag{23}$$

Behaviors, Lyapunov exponents values, Kaplan-Yorke dimensions and attractors of the new 5-D system (1) for different values of parameter d are summarized in Table 2.

IV. MULTISTABILITY AND COEXISTENCE OF ATTRACTORS

Multistability or coexisting attractors is a nonlinear phenomenon that means two or more different attractors generate simultaneously from different initial points [38], [39], [40]. By using numerical simulations, we found that the new 5-D system (1) is rich in coexisting attractors. The 5-D system (1) displays coexistence of two periodic attractors, two chaotic attractors or two hyperchaotic attractors for different choices of parameter values.

Since the 5-D system (1) is invariant under the coordinates transformation

$$(z_1, z_2, z_3, z_4, z_5) \mapsto (-z_1, -z_2, z_3, -z_4, -z_5),$$

the appearance of coexisting attractors may occur if we make the appropriate selection of initial points.

Let $Z_0 = (1, 1, 1, 1, 1)$ and $W_0 = (-1, -1, 1, -1, -1)$ be two different initial points for the new 5-D system (1), where we represent the state orbit corresponding to Z_0 as a blue color orbit and the state orbit corresponding to W_0 as a red color orbit.

Fix the parameters as $a = 40$, $b = 8$, $c = 16$ and $d = 12$. Then the 5-D system (1) displays two coexisting periodic attractors as shown in Figure 11 (a), where the blue attractor starts from Z_0 and the red attractor starts from W_0.

TABLE 2. Dynamics, Lyapunov exponents and Kaplan-Yorke Dimension of the 5-D System (1) versus its parameters.

Dynamics	Parameters				Bifurcation Parameter	Lyapunov Exponents					D_{KY}	Attractor
	a	b	c	d		LE_1	LE_2	LE_3	LE_4	LE_5		
Point	40	$[9, 14.5]$	16	12	$b = 10$	-0.198	-0.204	-1.332	-1.412	-48.511	0	Fig. 6 (b)
Periodic	$[0, 18.5]$, $[19.2, 20]$	90	16	12	$a = 12$	0	-0.117	-0.118	-11.874	-11.898	0	Fig. 4 (a)
	40	$[0, 9]$	16	12	$b = 4$	0	-0.475	-0.489	-7.092	-43.936	0	Fig. 6 (a)
	40	90	16	$[0, 1.1]$	$d = 0.7$	0	-0.580	-0.583	-1.280	-38.257	0	Fig. 10 (a)
Chaotic	$[18.5, 19.2]$, $[20, 20.4]$	90	16	12	$a = 19$	0.011	0	-0.252	-3.447	-27.307	2.044	Fig. 4 (b)
	40	90	$[0, 1.4]$	12	$c = 0.3$	12.175	0	-0.010	-0.017	-64.141	4.189	Fig. 8 (a)
Hyperchaotic	$[20.4, 32]$	90	16	12	$a = 25$	10.366	0.039	0	-0.020	-47.382	4.219	Fig. 4 (c)
	$[32, 40]$	90	16	12	$a = 39.8$	11.862	0.041	0.033	0	-63.706	4.187	Fig. 4 (d)
	40	$[14.5, 19.6]$, $[23.5, 26.5]$	16	12	$b = 16$	0.224	0.127	0	-1.246	-51.102	3.282	Fig. 6 (c)
	40	$[19.6, 23.5]$, $[26.5, 90]$	16	12	$b = 40$	4.220	0.172	0.112	0	-56.499	4.080	Fig. 6 (d)
	40	90	$[1.4, 6]$	12	$c = 2$	12.122	0.018	0	-0.013	-64.103	4.189	Fig. 8 (b)
	40	90	$[6, 20]$	12	$c = 20$	11.783	0.083	0.031	0	-63.867	4.186	Fig. 8 (c)
	40	90	16	$[1.1, 7]$	$d = 4$	4.868	0.046	0	-0.035	-48.856	4.100	Fig. 10 (b)
	40	90	16	$[7, 15]$	$d = 14$	12.388	0.047	0.017	0	-66.420	4.187	Fig. 10 (c)

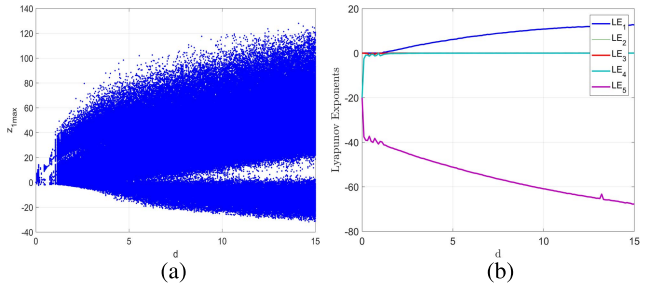

(a) (b)

FIGURE 9. Bifurcation diagram (a) and Lyapunov exponents spectrum (b) of the new 5-D hyperchaotic system (1) when $a = 40$, $b = 90$, $c = 16$ and $d \in [0, 15]$.

Fix the parameters as $a = 20.3$, $b = 90$, $c = 16$ and $d = 12$. Then the 5-D system (1) displays two coexisting chaotic attractors as shown in Figure 11 (b) starting from the initial points Z_0 (blue) and W_0 (red), respectively. The two coexisting chaotic attractors are characterized by the following values of Lyapunov exponents:

$$\begin{cases} LE_1 &= 0.219 \\ LE_2 &= 0 \\ LE_3 &= -0.096 \\ LE_4 &= -1.008 \\ LE_5 &= -31.414 \end{cases} \tag{24}$$

Fix the parameters as $a = 40$, $b = 15$, $c = 16$ and $d = 12$. Then the 5-D system (1) displays two coexisting

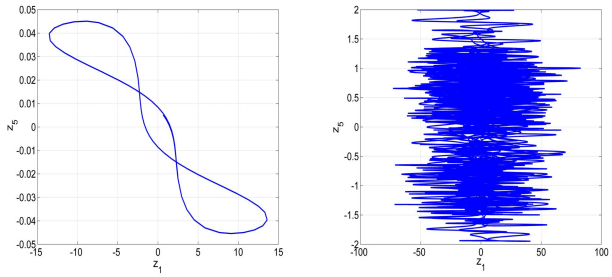

(a) $d = 0.7$, periodic (b) $d = 4$, hyperchaotic

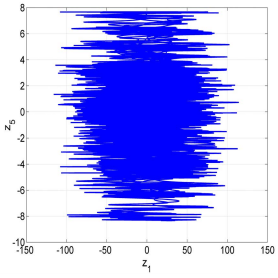

(c) $d = 14$, hyperchaotic

FIGURE 10. 2-D plots of the new 5-D hyperchaotic system (1) in the (z_1, z_5) -plane for $a = 40$, $b = 90$, $c = 16$ and different values of d.

hyperchaotic attractors as shown in Figure 11 (c) starting from the initial points Z_0 (blue) and W_0 (red), respectively. The two coexisting hyperchaotic attractors are characterized

by the following values of Lyapunov exponents:

$$\begin{cases} LE_1 & = 0.251 \\ LE_2 & = 0.078 \\ LE_3 & = 0 \\ LE_4 & = -1.576 \\ LE_5 & = -50.744 \end{cases} \tag{25}$$

Fix the parameters as $a = 40$, $b = 41$, $c = 16$ and $d = 12$. Then the 5-D system (1) displays two coexisting hyperchaotic attractors as shown in Figure 11 (d) starting from the initial points Z_0 (blue) and W_0 (red), respectively. The two coexisting hyperchaotic attractors are characterized by the following values of Lyapunov exponents:

$$\begin{cases} LE_1 & = 4.372 \\ LE_2 & = 0.176 \\ LE_3 & = 0.088 \\ LE_4 & = 0 \\ LE_5 & = -56.631 \end{cases} \tag{26}$$

V. OFFSET BOOSTING CONTROL

Offset boosting control means that the amplitude of the system can be flexibly controlled after introducing a control parameter in one of the states. The offset boosting does not change the qualitative behavior of the system dynamics but rather moves the attractor from its position to another one in a positive direction or negative direction according to the value of control parameter chosen. Since the fifth state variable of the 5-D hyperchaotic system (1), z_5, only appears in the fourth equation, the new 5-D system is a variable-boosting hyperchaotic system, where z_5 can be controllable. Hence,z_5 can be boosted via substituting z_5 by $z_5 + p$.

For offset-boosting control, the 5-D hyperchaotic system (1) can be rewritten as:

$$\begin{cases} \dot{z}_1 & = a(z_2 - z_1) + z_2 z_3 + z_4 \\ \dot{z}_2 & = z_1(b - z_3) + cz_4 \\ \dot{z}_3 & = z_1^2 + z_1 z_2 - dz_3 \\ \dot{z}_4 & = -z_2 + (z_5 + p) \\ \dot{z}_5 & = -z_4 \end{cases} \tag{27}$$

where p is an offset-boosting controller.

When we take the parameter values as $(a, b, c, d) = (40, 90, 16, 12)$ and initial state as $Z_0 = (1, 1, 1, 1)$, the offset boosted hyperchaotic attractors can be obtained for the 5-D system (27) as shown in Figure 12.

Various phase portraits of the hyperchaotic attractors boosted on different values of p in the (z_2, z_5) plane are plotted in Figure 12 (a). The hyperchaotic attractor of the 5-D system (27) is boosted in the positive direction for a negative value of p, while the attractor is boosted in a negative direction for a positive value of p. Consequently, the hyperchaotic

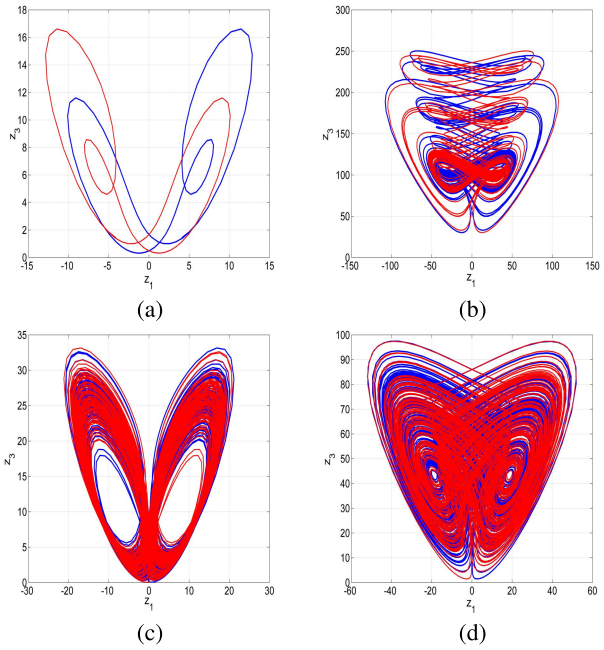

FIGURE 11. 2-D Matlab plots of the new 5-D hyperchaotic system (1) in the (z_1, z_3) -plane: (a) coexisting periodic attractors, (b) coexisting chaotic attractors, (c) coexisting hyperchaotic attractors with two positive LEs and (d) coexisting hyperchaotic attractors with three positive LEs.

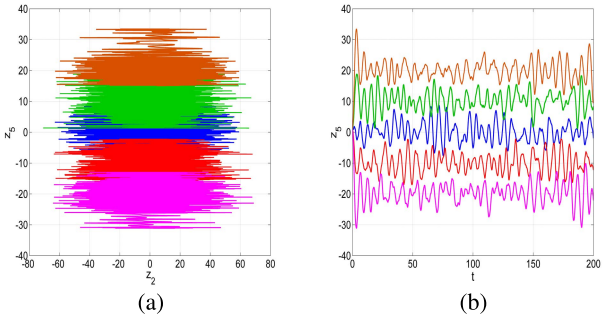

FIGURE 12. Offset-boosting control of the 5-D system (27) with different values of parameter p, $p = 0$ (blue), $p = 10$ (red), $p = -10$ (green), $p = 20$ (magenta) and $p = -20$ (brown):: (a) (z_2, z_5)-hyperchaotic attractors and (b) time-plot of the state z_5.

signal z_5 can be boosted from a bipolar hyperchaotic signal to a unipolar hyperchaotic signal as shown in Figure 12 (b). This special feature of offset boosting has a great application in secure communication and other fields of engineering.

VI. ELECTRONIC CIRCUIT IMPLEMENTATION OF THE NEW 5-D HYPERCHAOTIC SYSTEM

The analog circuit of the proposed 5-D hyperchaotic system (1) is implemented by adopting capacitors, resistors, operational amplifiers TL082CD and analog multipliers AD633JN. The circuit design of the 5-D hyperchaotic system is given in Figure 1. Electronic circuit implementation of the hyperchaotic system is designed in MultiSim (Version 13.0) for the parameters $a = 40$, $b = 90$, $c = 16$ and $d = 15$ with the initial condition $Z(0) = (1, 1, 1, 1, 1)$.

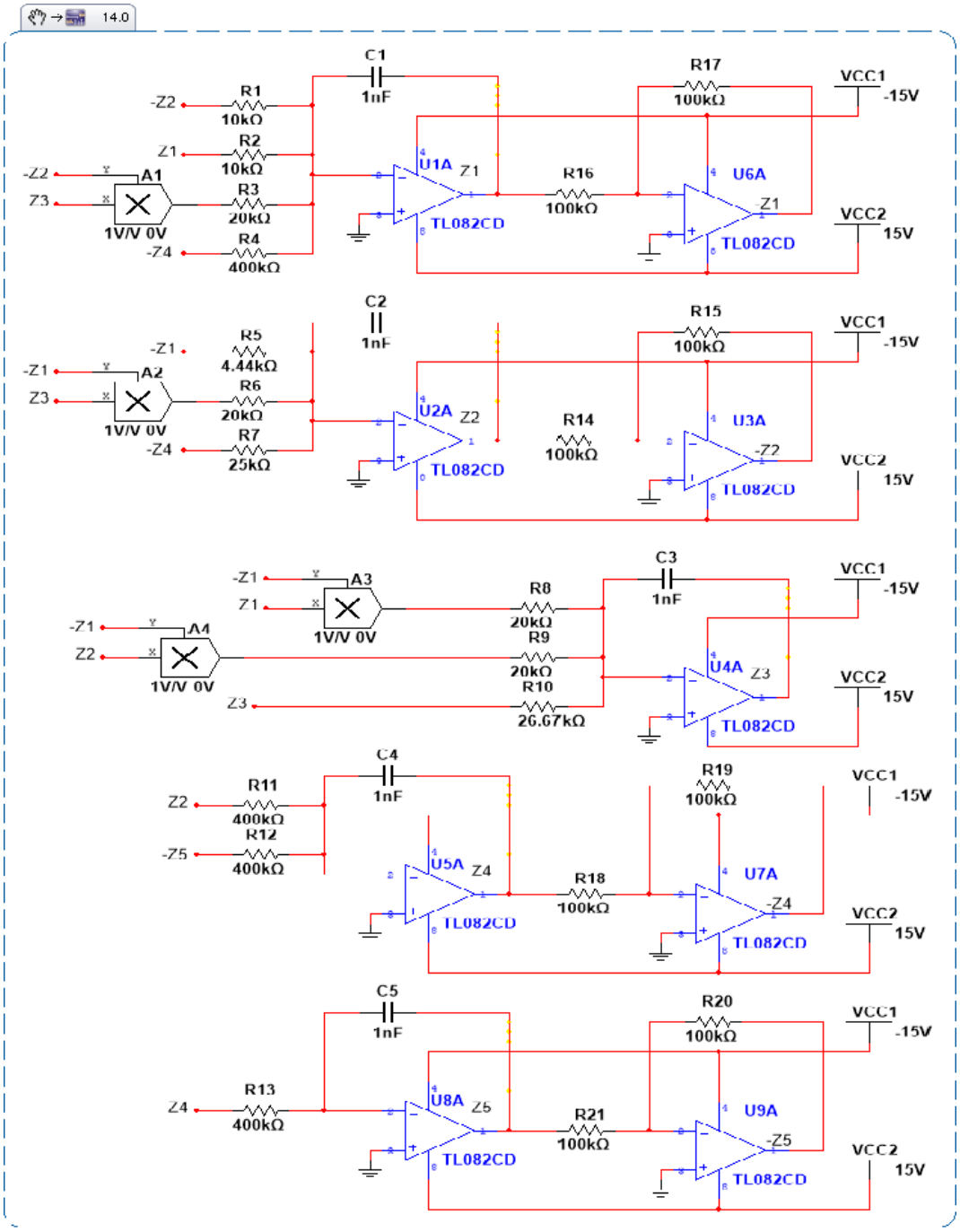

FIGURE 13. Schematic diagram of the electronic circuit of the 5-D hyperchaotic system (30).

For circuit implementation, we rescale the state variables of the hyperchaotic system (1) as follows:

$$\begin{cases} Z_1 &= \frac{1}{2}z_1 \\ Z_2 &= \frac{1}{2}z_2 \\ Z_3 &= \frac{1}{2}z_3 \\ Z_4 &= z_4 \\ Z_5 &= z_5 \end{cases} \tag{28}$$

The rescaled 5-D hyperchaotic system is given below:

$$\begin{cases} \dot{Z}_1 &= a(Z_2 - Z_1) + 2Z_2Z_3 + Z_4 \\ \dot{Z}_2 &= Z_1(b - 2Z_3) + cZ_4 \\ \dot{Z}_3 &= 2Z_1^2 + 2Z_1Z_2 - dZ_3 \\ \dot{Z}_4 &= -Z_2 + Z_5 \\ \dot{Z}_5 &= -Z_4 \end{cases} \tag{29}$$

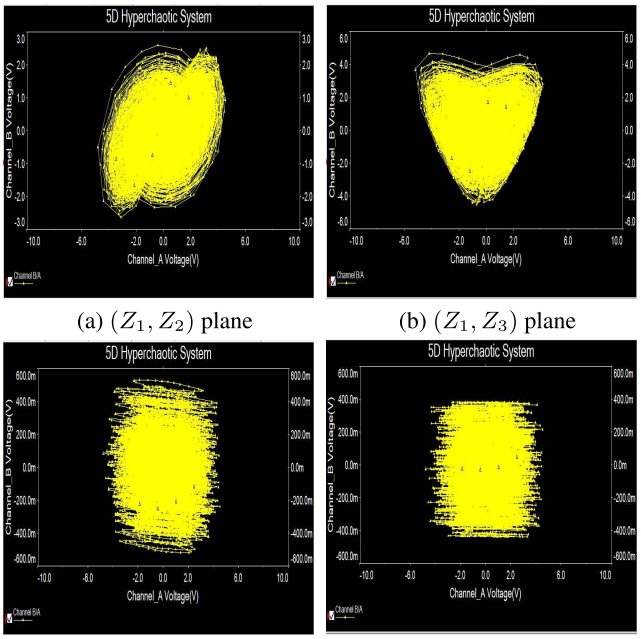

(a) (Z_1, Z_2) plane (b) (Z_1, Z_3) plane

(c) (Z_1, Z_4) plane (d) (Z_1, Z_5) plane

FIGURE 14. *2D* signal plots of the 5-D hyperchaotic circuit (30) using MultiSim circuit simulation.

Applying the Kirchhoff laws, the circuit presented in Figure 13 is described by the following:

$$\begin{cases} C_1\dot{Z}_1 &= \frac{1}{R_1}Z_2 - \frac{1}{R_2}Z_1 + \frac{1}{10R_3}Z_2Z_3 + \frac{1}{R_4}Z_4 \\ C_2\dot{Z}_2 &= \frac{1}{R_5}Z_1 - \frac{1}{10R_6}Z_1Z_3 + \frac{1}{R_7}Z_4 \\ C_3\dot{Z}_3 &= \frac{1}{10R_8}Z_1^2 + \frac{1}{10R_9}Z_1Z_2 - \frac{1}{R_{10}}Z_3 \\ C_4\dot{Z}_4 &= -\frac{1}{R_{11}}Z_2 + \frac{1}{R_{12}}Z_5 \\ C_5\dot{Z}_5 &= -\frac{1}{R_{13}}Z_4 \end{cases} \tag{30}$$

Here, Z_1, Z_2, Z_3, Z_4 and Z_5 correspond to the voltages on the integrators $U1A$, $U2A$, $U4A$, $U5A$, $U8A$, respectively. The values of resistors are considered as

$$R_1 = R_2 = 10\,k\Omega \tag{31}$$
$$R_3 = R_6 = R_8 = R_9 = 20\,k\Omega \tag{32}$$
$$R_4 = R_{11} = R_{12} = R_{13} = 400\,k\Omega \tag{33}$$
$$R_5 = 4.44\,k\Omega, R_7 = 25\,k\Omega, R_{10} = 26.67\,k\Omega \tag{34}$$
$$R_{14} = R_{15} = R_{16} = R_{17} = 100\,k\Omega \tag{35}$$
$$R_{18} = R_{19} = R_{20} = R_{21} = 100\,k\Omega \tag{36}$$

The capacitors are selected as

$$C_1 = C_2 = C_3 = C_4 = C_5 = 1\,nF. \tag{37}$$

MultiSim outputs of the 5-D hyperchaotic system (refsec-circuit-trans-eqn2) are presented in Figure 14, which agree with the MATLAB outputs of the new 5-D hyperchaotic system (1) shown in Figure 1.

VII. FPGA IMPLEMENTATION OF THE 5-D HYPERCHAOTIC SYSTEM

The FPGA is a hardware circuit allowing programmability to carry out both logical operations and arithmetic operations. Among its advantages is the great flexibility for fast prototyping and low development cost applications. In the case of chaotic systems, the FPGA implementation requires determining a numerical method and the step-size h to reach the maximum operating frequency. In this manner, the new 5-D chaotic system with three positive LEs, can be solved by applying one-step numerical methods with an appropriate h, as done in [41], where it is mentioned that using a high value of h helps to increase the operating frequency of chaotic/hyperchaotic systems. After selecting a numerical method, one can emulate the chaotic system in an FPGA as already done in [42], [43], [44], [45], [46], [47]. If the chaotic system has different parameter values to be tested, the FPGA is appropriate to reconfigure or reprogram the values.

The main difference in FPGA implementations of chaotic systems is mainly measured by the use of hardware resources, which are often divided into configurable logic cells, random access memory (RAM) block, DSP slices, and transceivers. Some multipliers are embedded into the FPGA but in some cases they can be designed using shift registers and adders, as shown in [48], where single-constant-multiplier (SCM) blocks are implemented to generate multi-scroll chaotic attractors. In that work, the authors also show the application of Forward Euler (FE) and Runge Kutta (RK) methods for the FPGA implementation of a chaotic system based on saturated nonlinear function series. In this work, we show the application of FE and Trapezoidal rule. The former is an explicit numerical method and the second an implicit one, which requires the use of an implicit method, as shown below.

The FE method is based on (38), which current iteration index $n+1$ depends on one-step at iteration n, and is evaluated by $f(x_n, t_n)$. Applying this numerical method, the discretized equations of the new 5-D hyperchaotic system are given by (39), from which one can identify arithmetic operations that can be implemented by using multipliers, adders and subtractors.

$$x_{n+1} = x_n + hf(x_n, t_n) \tag{38}$$
$$\begin{aligned} z1_{n+1} &= z1_n + h[a(z2_n - z1_n) + z2_n z3_n + z4_n] \\ z2_{n+1} &= z2_n + h[z1_n(b - z3_n) + cz4_n] \\ z3_{n+1} &= z3_n + h[z1_n z1_n + z1_n z2_n - dz3_n] \\ z4_{n+1} &= z4_n + h[-z2_n + z5_n] \\ z5_{n+1} &= z5_n + h[-z4_n] \end{aligned} \tag{39}$$

The second numerical method applied herein is the Trapezoidal rule whose iterative equation is given in (40). As this method requires of evaluating the function at the same current index, i.e. $f(x_{n+1}, t_{n+1})$, we apply FE to evaluate this value. In this manner, the discretized equations are given in (41), where one can see that more arithmetic operations are needed, so that it requires more resources in the

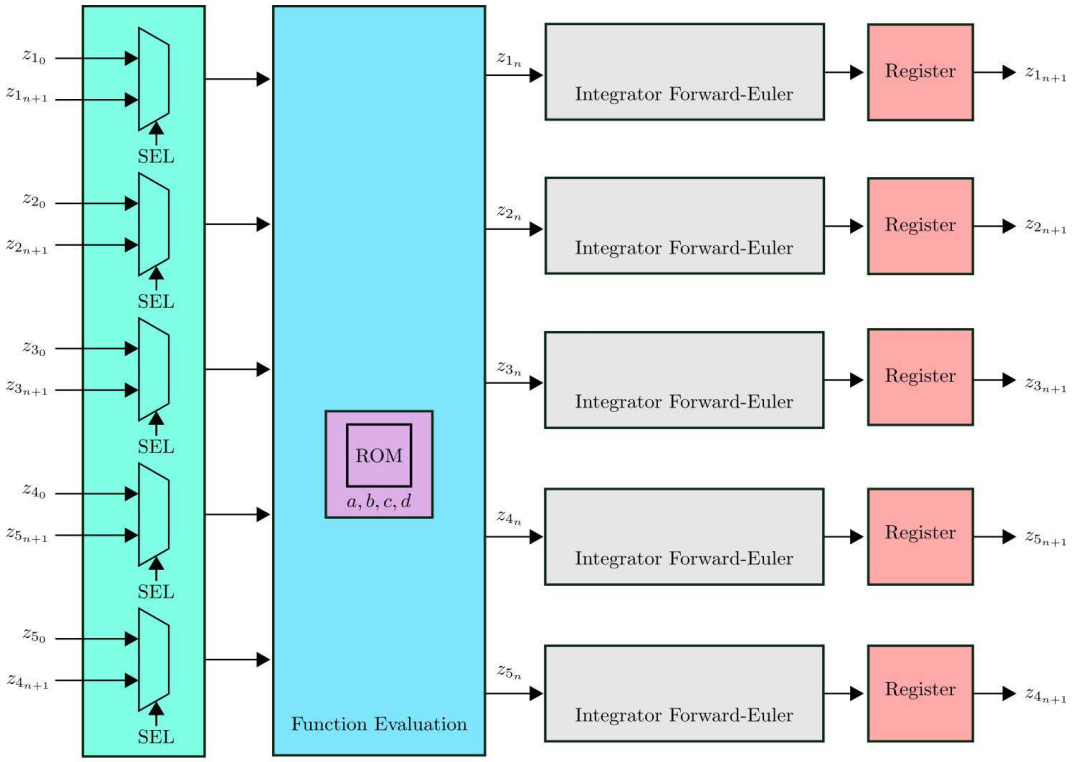

FIGURE 15. Block diagram of the new 5-D hyperchaotic system applying Forward Euler method.

FPGA implementation.

$$x_{n+1} = x_n + \frac{h}{2}[f(x_n, t_n) + f(x_{n+1}, t_{n+1})] \tag{40}$$

$$\begin{aligned}
z1_{n+1} &= z1_n + \frac{h}{2}\{[a(z2_n - z1_n) + z2_n z3_n + z4_n] \\
&\quad + [a(z2_{n+1} - z1_{n+1}) + z2_{n+1} z3_{n+1} + z4_{n+1}]\} \\
z2_{n+1} &= z2_n + \frac{h}{2}\{[z1_n(b - z3_n) + cz4_n] \\
&\quad + [z1_{n+1}(b - z3_{n+1}) + cz4_{n+1}]\} \\
z3_{n+1} &= z3_n + \frac{h}{2}\{[z1_n z1_n + z1_n z2_n - dz3_n] \\
&\quad + [z1_{n+1} z1_{n+1} + z1_{n+1} z2_{n+1} - dz3_{n+1}]\} \\
z4_{n+1} &= z4_n + \frac{h}{2}\{[-z2_n + z5_n] + [-z2_{n+1} + z5_{n+1}]\} \\
z5_{n+1} &= z5_n + \frac{h}{2}\{[-z4_n] - [z4_{n+1}]\}
\end{aligned} \tag{41}$$

The synthesis of all the blocks to perform the arithmetic operations can be designed by adopting a computer arithmetic based on fixed-point format. In this case, each real value is represented with the format 16.48 (64 bits), using one bit for the sign, 15 bit to represent the integer part, and 64 for the fractional part. It is worthy mentioning that this 16.48 format is established after observing the amplitudes of the state variables. For example, simulation results for this new 5-D hyperchaotic system taking into account all multiplications among state variables, provide the amplitude range approximately between [−24000,23500], so that 15 bits are enough to represent up to 32768 in the integer part, and one bit is used for the sign, given 16 bits in the format 16.48. The high level description of the main blocks for the implementation of the new 5-D hyperchaotic system, is shown in Fig. 17. As one sees, the values of the coefficients a, b, c, d are stored in a read only memory (ROM), which can be reprogrammed if they are optimized. The iterations are controlled by a state machine to process the values are iteration n to give the values at current iteration $n + 1$. Those results at $n + 1$ are always available at the registers and feedback through the multiplexer blocks, which also control the initial conditions. The implementation applying the Trapezoidal method is performed in a similar manner, but it requires of an explicit method, as already shown in [48] applying RK method and FE as predictor. In this manner, the hardware resources are listed in Table 3. One can appreciate that the Trapezoidal method doubles the logic elements, as one can infer observing (40) and (41). The requirement of multipliers also increase in the Trapezoidal method. Finally, as the state machine is designed to control the same clock cycles, the latency is the same.

VIII. APPLICATION TO IMAGE CRYPTOSYSTEM

Data security acts a vital role in present days, in which digital images represent the familiar model of representing the data.

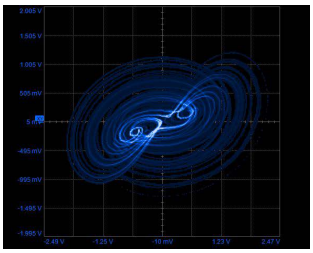

(a) z_1 vs z_2 view

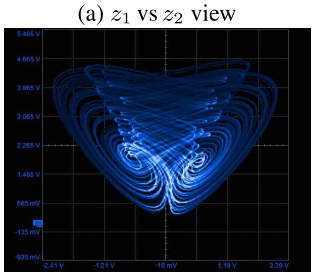

(b) z_1 vs z_3 view

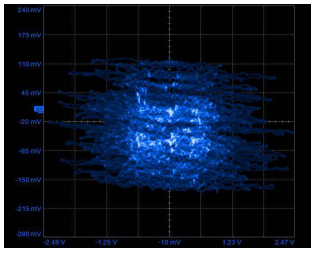

(c) z_1 vs z_4 view

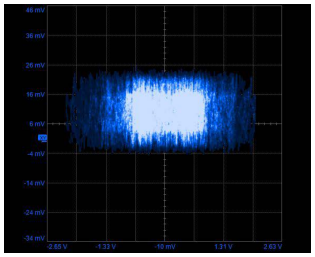

(d) z_1 vs z_5 view

FIGURE 16. Experimental attractors of the new 5-D hyperchaotic system from the FPGA implementation with $h = 0.001$. (a) $z_1 - z_2$ view, (b) $z_1 - z_3$ view, (c) $z_1 - z_4$ view and (d) $z_1 - z_5$ view.

TABLE 3. Hardware resources for the implementation of the new 5-D hyperchaotic system by using the FPGA Basys 3 Xilinx Artix-7 XC7A35T-ICPG236C, applying FE and Trapezoidal methods, and setting $h = 0.0001$.

Resources	Forward Euler	Trapezoidal	Available
Logic Elements	4200	8350	20,800
Registers	350	350	41,600
Multipliers	11	15	–
Max Freq. (MHz)	50	50	50
Cloock cycles by Iteration	2	2	-
Latency(ns)	40	40	-

Chaotic maps are considered the backbone of designing modern image encryption mechanism. In this section, we adapt the hyperchaotic system to be iterative and applicable in

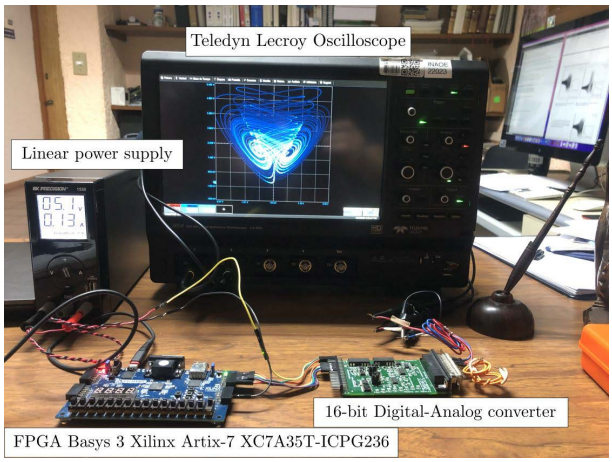

FIGURE 17. Experimental setup to observe the experimental attractors of the new 5-D hyperchaotic system using a FPGA Basys 3 Xilinx Artix-7 XC7A35T-ICPG236, a DAC, a linear power supply and an oscilloscope.

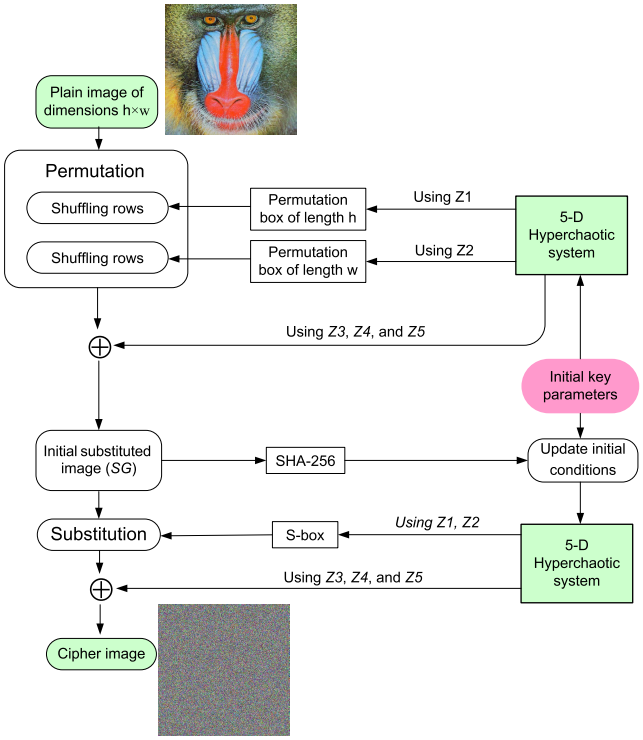

FIGURE 18. Outline of the encryption algorithm for the suggested cryptosystem.

modern security proposes as expressed in Eq. (42).

$$\begin{cases} z(1)_{i+1} = (a\,(z(2)_i - z(1)_i) + z(2)_i z(3)_i + z(4)_i)\ mod\, 1 \\ z(2)_{i+1} = (z(1)_i\,(b - z(3)_i) + cz(4)_i)\ mod\, 1 \\ z(3)_{i+1} = \left(z(1)_i^2 + z(1)_i z(2)_i - dz(3)_i\right)\ mod\, 1 \\ z(4)_{i+1} = (-z(2)_i + z(5)_i)\ mod\, 1 \\ z(5)_{i+1} = (-z(4)_i)\ mod\, 1 \end{cases} \tag{42}$$

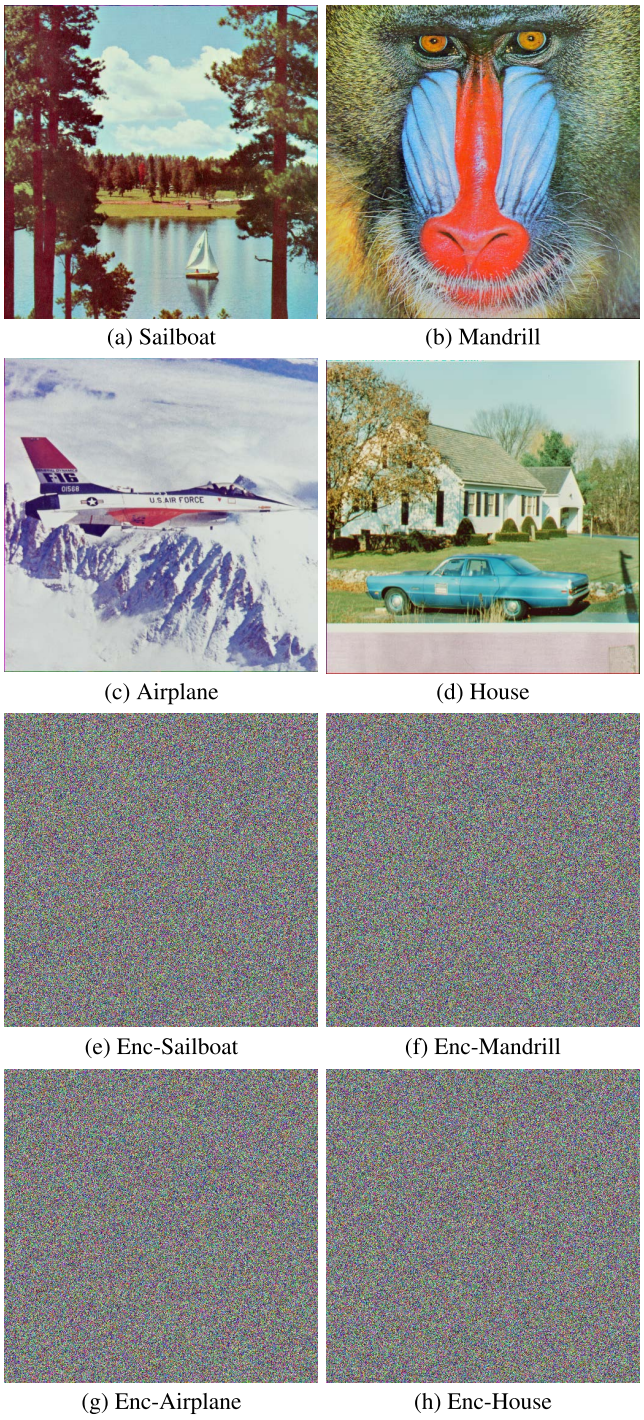

FIGURE 19. Dataset of images and its resulted cipher images using our cryptosystem.

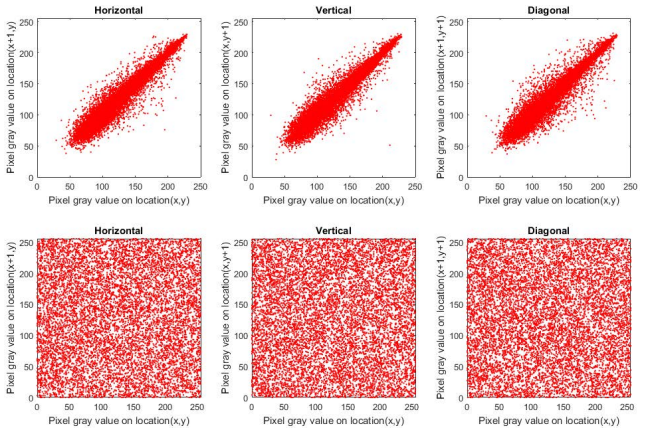

FIGURE 20. Correlation distribution in each direction for the red channel of Sailboat image, where the first row plots the distribution for the plain version while the last row plots the distribution for the encrypted version.

A. ENCRYPTION PROCEDURE

In this section, we present a new color image encryption mechanism using the presented 5-D hyperchaotic map (42). In the proposed algorithm, the hyperchaotic system is employed to generate five chaotic sequences (*Z1*, *Z2*, *Z3*, *Z4*, and *Z5*), in which the first two chaotic sequences (*Z1* and *Z2*), are utilized to construct two permutation boxes for permutating the plain image (*PG*), then the other three sequences (*Z3*, *Z4*, and *Z5*) are operated to substitute the permutated image (*PrG*). To ensure the plain image sensitivity of our encryption technique, SHA256 hashing algorithm is applied on the substituted image (*SG*), then utilizes the hash value for updating the initial values ($z(1)_0$, $z(2)_0$, $z(3)_0$, $z(4)_0$, and $z(5)_0$) of the presented hyperchaotic map. Note that the generated hash value does not depend only on the plain image (*PG*) but also on the primary conditions and control parameters ($z(1)_0$, $z(2)_0$, $z(3)_0$, $z(4)_0$, $z(5)_0$, a, b, c, and d) of the hyperchaotic system. The updated initial values ($z(1)_u$, $z(2)_u$, $z(3)_u$, $z(4)_u$, and $z(5)_u$) are utilized to iterate the hyperchaotic system for generating another five chaotic sequences, in which the first two chaotic sequences are utilized to construct a substitution box (S-box), then the other three sequences and the generated S-box are utilized to construct the final cipher image. For more illustration, the sketch of the encryption algorithm is outlined in Figure 18 and the details of the encryption technique are given in Algorithm 1.

B. SECURITY ANALYSIS

The quality of a cryptosystem to encrypt a document depends essentially on its performance and resist security attacks such as differential cryptanalysis, statistical cryptanalysis, brute force attacks, etc. These fundamental effects are investigated in this section.

To assess the proposed encryption approach, a personal computer with 4GB of RAM and Intel $Core^{TM}$ 2 Duo CPU 3GHz and equipped with MATLAB R2016b. The experimental dataset of images is taken from SIPI database [49] and labeled as Sailboat, Mandrill, Airplane, and House (Figure 19), in which the dimensions of each color image is 512×512. The initial key utilized for iterating the hyperchaotic system are set as $z(1)_0 = 0.8531$, $z(2)_0 = 0.3427$,

Algorithm 1 Image Encryption Process

parameter: $z(1)_0$, $z(2)_0$, $z(3)_0$, $z(4)_0$, $z(5)_0$, a, b, c, and d
Input: Plain image(PG)
Output: Cipher image (CG), hash value

$[h\ \ w\ \ color] \leftarrow size(PG)$// Obtain the plain image dimensions
$[Z1\ \ Z2\ \ Z3\ \ Z4\ \ Z5\ ] \leftarrow HyperChaoticSystem(z(1)_0, z(2)_0, z(3)_0, z(4)_0, z(5)_0, a, b, c, d, h \times w)$
// iterating system (42) for h × w times
// Constructing permutation boxes
$SR \leftarrow Sort(Z1(1:h))$ // order the numbers of Z1(1:h) in ascending order
$Pbox1 \leftarrow index(Z1(1:h), SR)$ // Take the index of every element of Z1(1:h) in SR
$SC \leftarrow Sort(Z2(1:w))$
$Pbox2 \leftarrow index(Z2(1:w), SC)$
// Permutation process
$PrG1(Pbox1(p), :, :) \leftarrow PG(p, :, :) \quad for \quad p = 1, 2, \ldots, h$// Shuffling rows of PG
$PrG(:, Pbox2(p), :) = PrG1(:, p, :) \quad for \quad p = 1, 2, \ldots, w$// Shuffling columns of PrG1
$Key(:, :, 1) \leftarrow round(Z3 \times 10^{16}) \mod 256$// Converting Z3 sequence into integers
$Key(:, :, 2) \leftarrow round(Z4 \times 10^{16}) \mod 256$
$Key(:, :, 3) \leftarrow round(Z5 \times 10^{16}) \mod 256$
$SG \leftarrow PrG \oplus key$ // First pixel substitution
$HV \leftarrow SHA256(SG)$// Get the hash value for SG image
$v \leftarrow uint8(HV)$// Transforming each 8-bit into an integer
$V1 \leftarrow (v_1 \oplus v_2 \oplus \cdots \oplus v_6)/256$
$V2 \leftarrow (v_7 \oplus v_8 \oplus \cdots \oplus v_{12})/256$
$V3 \leftarrow (v_{13} \oplus v_{14} \oplus \cdots \oplus v_{18})/256$
$V4 \leftarrow (v_{19} \oplus v_{20} \oplus \cdots \oplus v_{25})/256$
$V5 \leftarrow (v_{26} \oplus v_{27} \oplus \cdots \oplus v_{32})/256$
// Updating initial values of $(z(1)_0,\ z(2)_0,\ z(3)_0,\ z(4)_0,\ z(5)_0)$
$z(1)_u \leftarrow (z(1)_0 + V1)/2$
$z(2)_u \leftarrow (z(2)_0 + V2)/2$
$z(3)_u \leftarrow (z(3)_0 + V3)/2$
$z(4)_u \leftarrow (z(4)_0 + V4)/2$
$z(5)_u \leftarrow (z(5)_0 + V5)/2$
$[Z1\ \ Z2\ \ Z3\ \ Z4\ \ Z5\ ] \leftarrow HyperChaoticSystem(z(1)_u, z(2)_u, z(3)_u, z(4)_u, z(5)_u, a, b, c, d, h \times w)$
// Constructing a substitution box
$Y \leftarrow Z1(1:256) + Z2(1:256)$
$SB \leftarrow Sort(Y)$
$Sbox \leftarrow index(Y, SB)$
for $p \leftarrow 1$ *to* h **do**
  for $q \leftarrow 1$ *to* w **do**
    for $r \leftarrow 1$ *to* $color$ **do**
      $CG1(p, q, r) \leftarrow Sbox(SG(p, q, r) + 1)$
$KeyFinal(:, :, 1) \leftarrow round(Z3 \times 10^{16}) \mod 256$
$KeyFinal(:, :, 2) \leftarrow round(Z4 \times 10^{16}) \mod 256$
$KeyFinal(:, :, 3) \leftarrow round(Z5 \times 10^{16}) \mod 256$
$CG \leftarrow CG1 \oplus KeyFinal$ // Final cipher image

$z(3)_0 = 0.6482$, $z(4)_0 = 0.8356$, $z(5)_0 = 0.2943$, $a = 40$, $b = 90$, $c = 16$, and $d = 15$.

1) ANALYSIS OF CORRELATION COEFFICIENTS

To evaluate the meaningful of cipher images, the test of correlation coefficients is utilized, which can be stated mathematically as follows:

$$CC = \frac{\sum_{j=1}^{T} (c_j - \bar{c})(p_j - \bar{p})}{\sqrt{\sum_{j=1}^{T} (c_j - \bar{c})^2 \sum_{j=1}^{T} (p_j - \bar{p})^2}} \tag{43}$$

where c_j, p_j are refer to the values of adjoining pixels and T refers to the total number of adjoining pixel pairs in

TABLE 4. Results of *CC* for the tested dataset.

Image	Direction								
	Horizontal			Vertical			Diagonal		
	R	G	B	R	G	B	R	G	B
Sailboat	0.9565	0.9701	0.9699	0.9592	0.9728	0.9721	0.9474	0.9566	0.9549
Mandrill	0.8643	0.7771	0.8882	0.9185	0.8737	0.9106	0.8519	0.7474	0.8496
Airplane	0.9627	0.9701	0.9366	0.9723	0.9632	0.9621	0.9399	0.9399	0.9151
House	0.9589	0.9547	0.9753	0.9562	0.9412	0.9721	0.9238	0.9067	0.9511
Enc- Sailboat	0.0011	0.0005	0.0005	0.0004	-0.0002	0.0001	-0.0004	-0.0001	0.0002
Enc-Mandrill	-0.0006	0.0002	-0.0004	0.0010	0.0009	0.0013	-0.0005	-0.0002	-0.0006
Enc-Airplane	-0.0008	-0.0009	-0.0004	0.0004	-0.0006	-0.0001	-0.0007	0.0011	-0.0001
Enc-House	-0.0001	-0.0005	-0.0006	-0.0007	0.0005	0.0002	0.0002	0.0004	-0.0011

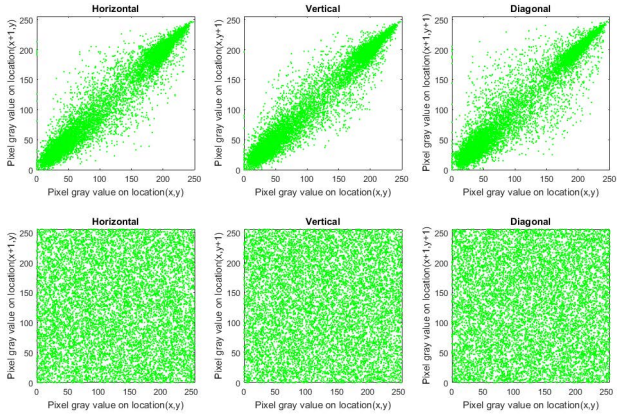

FIGURE 21. Correlation distribution in each direction for the green channel of Sailboat image, where the first row plots the distribution for the plain version while the last row plots the distribution for the encrypted version.

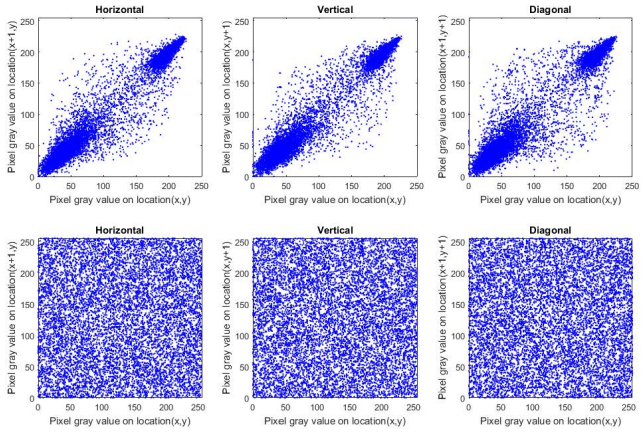

FIGURE 22. Correlation distribution in each direction for the blue channel of Sailboat image, where the first row plots the distribution for the plain version while the last row plots the distribution for the encrypted version.

each direction. Commonly, the values of *CC* for plain images are very near to one, while its values for cipher images with well-designed image cryptosystem are very near to zero. To calculate *CC* values for our cryptosystem, we selected randomly 10,000 pairs of neighboring pixels in each direction. Table 4 provides the outcomes for *CC*, in which *CC* values

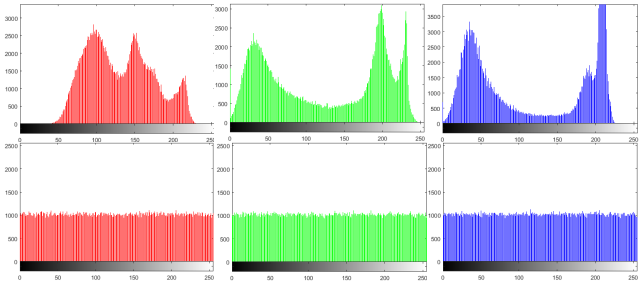

FIGURE 23. Histograms of Sailboat image before and after ciphering, where the histograms for the plain image are given in the first row and each dissimilar with each other while the plots of Enc-Sailboat image are provided in the last row and each similar with each other.

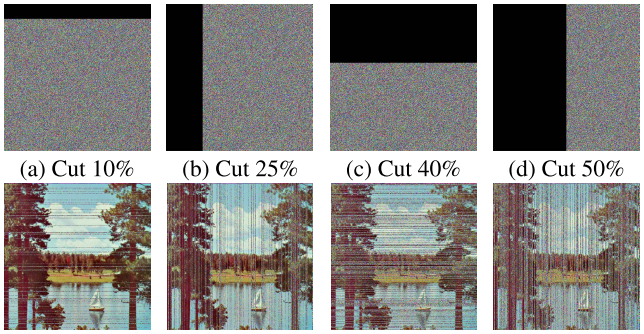

FIGURE 24. Results of data loss analysis, where the plain image is retrieved efficiently (last row) from the deficient encrypted image (first row) without losing information in the cut part.

for cipher images are very near to ideal value 0. As well, Figures 20, 21, and 22 display distributions for correlation coefficients in each direction for the plain Sailboat image and its analogous ciphered image. From the listed outcomes about *CC* values, no beneficial data was obtained concerning the cipher image by investigating *CC* results.

2) DIFFERENTIAL ANALYSIS

To estimate the plain image sensitivity for the presented cryptosystem, we utilized UACI "Unified Average Changing Intensity") and NPCR ("Number of Pixels Change Rate") test. UACI and NPCR are stated mathematically

TABLE 5. Results of UACI and NPCR testes.

Image	UACI	NPCR
Sailboat	33.47171%	99.61980%
Mandrill	33.45736%	99.61865%
Airplane	33.45881%	99 62158%
House	33 45842%	99.61561%

as follows:

$$NPCR = \frac{\sum_{m;n} D(m,n)}{T} \times 100\% \quad ,$$
$$D(m,n) = \begin{cases} 0 & if \;\; CG1(m,n) = CG2(m,n) \\ 1 & if \;\; CG1(m,n) \neq CG2(m,n) \end{cases} \tag{44}$$

$$UACI = \frac{1}{T}\left(\sum_{m,n} \frac{|CG1(m,n) - CG2(m,n)|}{256}\right) \times 100\% \tag{45}$$

where $CG1$, $CG2$ are two cipher images for one original image with modification in 1-bit, and T refers to the complete number of pixels. The outcomes of UACI and NPCR testes are displayed in Table 5 and confirm that the presented cryptosystem owns high sensitivity for slight pixel alterations in the plain image.

3) HISTOGRAM ANALYSIS

Histogram test is applied to evaluate the frequency of pixel values in an image, where histograms for different plain images are distinct from each other's, while histograms for cipher images generated from a well-designed cryptosystem ought to be similar with each other for resisting statistical attacks. Figure 23 parades the histograms of Sailboat image before and after ciphering, where the histograms for the plain image are dissimilar with each other whereas the plots of Enc-Sailboat image are similar with each other. However, we lack a quantifiable measure to identify the similarity of histograms such as the Chi-square test (χ^2) which can be described mathematically as follows:

$$\chi^2 = \sum_{j=0}^{255} \frac{(r_j - s)^2}{s} \tag{46}$$

here s points to the image size and r_j states the frequency of pixel value j. By assuming the significant level is $\alpha = 0.05$, then $\chi^2_\alpha(255) = 293.32$. For an image, when the χ^2 value is fewer than $\chi^2_\alpha(255)$, this refers that the given image holds a similar histogram distribution; else, the image owns a dissimilar distribution. The outcomes of Chi-square test are displayed in Table 6, in which all χ^2 values for all ciphered images is fewer than $\chi^2_\alpha(255)$. Thus, the presented cryptosystem has the ability to resist histogram analysis attacks.

TABLE 6. Outcomes of Chi-square test.

Image	χ^2 value		
	Red	Green	Blue
Sailboat	196697.3066	130154.7167	344571.5371
Mandrill	82839.7285	142808.0391	79942.6171
Airplane	678424.4921	682495.3828	1107858.0058
House	192029.6503	332540.1171	248006.8476
Enc-Sailboat	268.6152	252.8711	234.8750
Enc-Mandrill	242.7265	242.0820	246.8886
Enc-Airplane	256.1269	232.7500	218.4804
Enc-House	258.4160	248.5605	234.1093

TABLE 7. Outcomes of information entropy.

Image	Pristine	Cipher
Sailboat	7.7621696	7.9997482
Mandrill	7.7624361	7.9997781
Airplane	6.6639081	7.9997854
House	7.4857872	7.9997481

4) ENTROPY ANALYSIS

To assess the randomness of an image, information entropy test is applied, which can be given as follows:

$$E(X) = -\sum_{k=0}^{255} p(x_k) \log_2 (p(x_k)) \tag{47}$$

here $p(x_k)$ points to the probability of x_k. Any grey scale image has 2^8 probable values, accordingly the ideal value of entropy is equal to 8. Hence, the entropy value of the cipher images generated using a well-designed technique must be very near to the optimal value. The outcomes of the entropy test are displayed in Table 7, where all values for cipher images are very near to the ideal value. Therefore, the suggested cryptosystem has the ability to withstand statistical analysis originated from entropy attacks.

5) DATA LOSS ANALYSIS

Most telecommunication channels suffer from data loss attacks. Therefore, well-designed cryptosystems should have the ability to retrieve secret data from deficient cipher images. To assess the proposed cryptosystem contra these attacks, we cut out some slices of a cipher image, then attempt to decipher the deficient encrypted image. Figure 24 displays the outcomes of data loss attacks, where the original image is retrieved efficiently from the deficient encrypted image without losing information in the cut slice.

6) KEY SENSITIVITY ANALYSIS

Any cryptosystem has a secret key used in the ciphering and deciphering procedure. The utilized key must be sensitive to tiny modification in the secret key. To assess the key sensitivity of our cryptosystem, the cipher Enc-Sailboat image was deciphered many times with tiny alternations in the primary key parameters as stated in Figure 25.

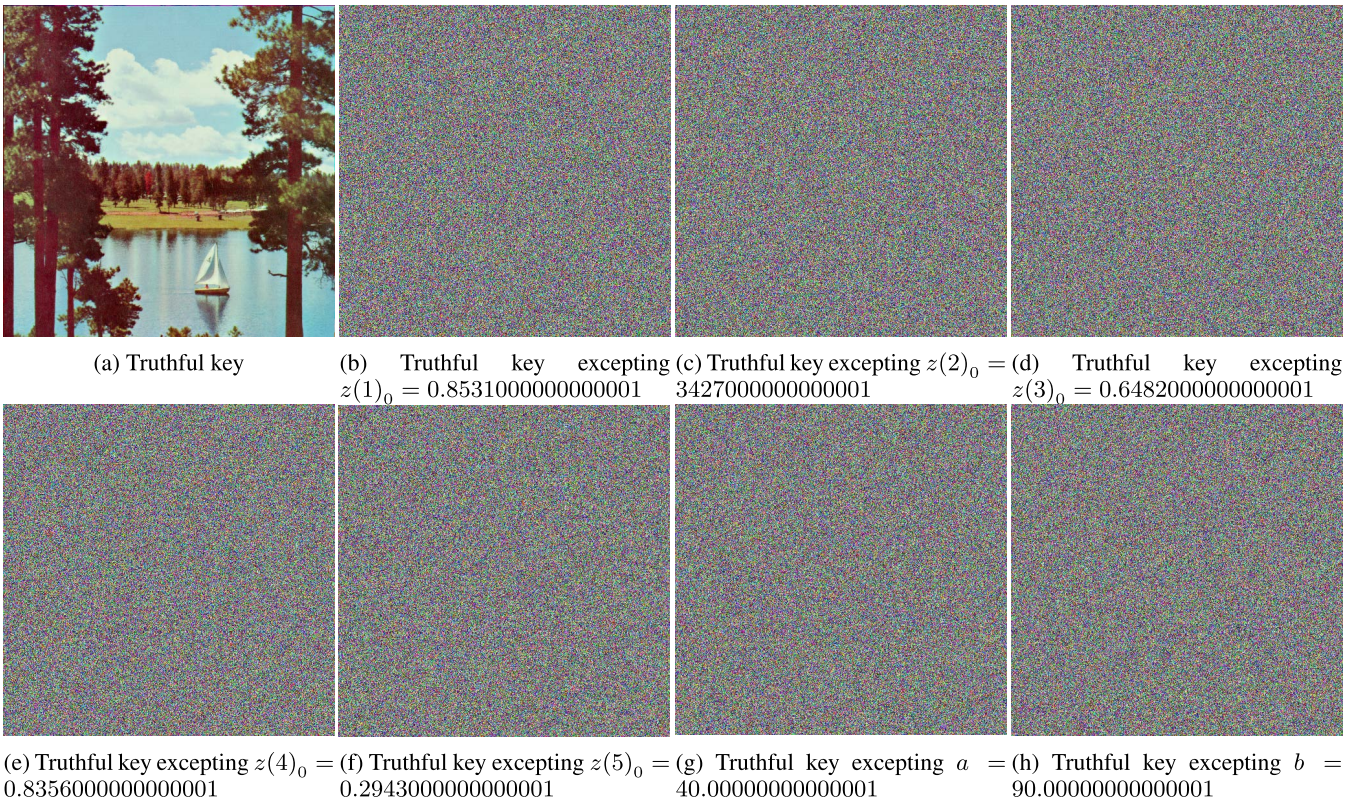

(a) Truthful key (b) Truthful key excepting $z(1)_0 = 0.8531000000000001$ (c) Truthful key excepting $z(2)_0 = 3427000000000001$ (d) Truthful key excepting $z(3)_0 = 0.6482000000000001$

(e) Truthful key excepting $z(4)_0 = 0.8356000000000001$ (f) Truthful key excepting $z(5)_0 = 0.2943000000000001$ (g) Truthful key excepting $a = 40.000000000000001$ (h) Truthful key excepting $b = 90.000000000000001$

FIGURE 25. Enc-Sailboat image deciphered many times with slight alternations in the primary key parameters.

TABLE 8. Simple comparison in average values of UACI, NPCR, Chi-square, entropy, and correlation.

Cryptosystem	UACI	NPCR	Chi-square	Entropy	Correlation		
					H	V	D
Proposed	33.462%	99.619%	244.7085	7.99976	-0.00005	0.00009	-0.00008
[25]	33.472%	99.622%	250.5122	7.99949	-0.00016	0.00002	0.00023
[11]	33.483%	99.613%	254.4314	7.99984	0.00018	-0.00002	0.00012
[50]	33.473%	99.600%	264.4174	7.99930	-0.00063	0.00083	-0.00034
[26]	33.440%	99.600%	257.3367	7.99700	-0.00970	-0.00870	0.00650

C. COMPARATIVE ANALYSIS

To prove that our cryptosystem possesses high efficiency and security compared to most recent encryption algorithms, Table 8 shows a simple comparison in average values of UACI, NPCR, Chi-square, entropy, and correlation. It is obvious that the presented cryptosystem is effective compared to other encryption algorithms.

IX. CONCLUSION

This work described the model of a new 5-D hyperchaotic system with three equilibrium points and deduced that the new hyperchaotic system has three positive Lyapunov exponents. Since the maximum positive Lyapunov exponent of the proposed hyperchaotic system is larger than twelve, we noted that the new hyperchaotic system is highly hyperchaotic. We also showed that the new 5-D hyperchaotic system exhibits multistability with coexisting attractors. Offset boosting control is also derived for the new 5-D hyperchaotic system. Using MultiSim, we designed an electronic circuit for the implementation of the new 5-D hyperchaotic system and present the circuit simulation results. The FPGA implementation of the new 5-D hyperchaotic system has been performed applying an explicit numerical method (FE) and an implicit one (Trapezoidal). We provided the discretized equations applying both methods to observe the arithmetic operations, so that the hardware resources given in Table 3 show that the Trapezoidal method doubles the logic elements, and requires more multipliers. Also, the experimental observation of the attractors show good agreement among FPGA implementation, circuit design and numerical simulations. Finally, the proposed 5-D hyperchaotic system can be utilized in designing reliable cybersecurity applications. As an example of the cryptographic application for the presented 5-D hyperchaotic map, we proposed a new color image cryptosystem, in which its experimental results proved its efficiency.

ACKNOWLEDGMENT

The author Aliyu Muhammed Awwal would like to thank the Postdoctoral Fellowship from the King Mongkut's University of Technology Thonburi (KMUTT), Thailand.

REFERENCES

[1] S. Yan, E. Wang, Q. Wang, X. Sun, and Y. Ren, "Analysis, circuit implementation and synchronization control of a hyperchaotic system," *Phys. Scripta*, vol. 96, no. 12, Dec. 2021, Art. no. 125257.

[2] Y. Bian and W. Yu, "A secure communication method based on 6-D hyperchaos and circuit implementation," *Telecommun. Syst.*, vol. 77, no. 4, pp. 731–751, Aug. 2021.

[3] J. Wang, W. Yu, J. Wang, Y. Zhao, J. Zhang, and D. Jiang, "A new six-dimensional hyperchaotic system and its secure communication circuit implementation," *Int. J. Circuit Theory Appl.*, vol. 47, no. 5, pp. 702–717, Mar. 2019.

[4] Z. Peng, W. Yu, J. Wang, Z. Zhou, J. Chen, and G. Zhong, "Secure communication based on microcontroller unit with a novel five-dimensional hyperchaotic system," *Arabian J. Sci. Eng.*, vol. 47, pp. 813–828, Mar. 2021.

[5] C. Xiu, J. Fang, and Y. Liu, "Design and circuit implementation of a novel 5D memristive CNN hyperchaotic system," *Chaos, Solitons Fractals*, vol. 158, May 2022, Art. no. 112040.

[6] X. Li, C. Zheng, X. Wang, Y. Cao, and G. Xu, "A novel five-dimensional memristive hyperchaotic system with extreme multistability," *J. Harbin Inst. Technol.*, vol. 54, no. 3, pp. 163–170, 2022.

[7] H. Alibraheemi, Q. Al-Gayem, and E. Hussein, "Four dimensional hyperchaotic communication system based on dynamic feedback synchronization technique for image encryption systems," *Int. J. Electr. Comput. Eng.*, vol. 12, no. 1, pp. 957–965, 2022.

[8] N. Khan and P. Muthukumar, "Transient chaos, synchronization and digital image enhancement technique based on a novel 5D fractional-order hyperchaotic memristive system," *Circuits, Syst., Signal Process.*, vol. 41, no. 4, pp. 2266–2289, Apr. 2022.

[9] J. V. N. Tegnitsap and H. B. Fotsin, "Multistability, transient chaos and hyperchaos, synchronization, and chimera states in wireless magnetically coupled VDPCL oscillators," *Chaos, Solitons Fractals*, vol. 158, May 2022, Art. no. 112056.

[10] Z. Wang, Z. Wei, K. Sun, S. He, H. Wang, Q. Xu, and M. Chen, "Chaotic flows with special equilibria," *Eur. Phys. J. Special Topics*, vol. 229, nos. 6–7, pp. 905–919, Mar. 2020.

[11] S. Vaidyanathan, A. Sambas, E. Tlelo-Cuautle, A. A. A. El-Latif, B. Abd-El-Atty, O. Guillen-Fernandez, K. Benkouider, M. A. Mohamed, M. Mamat, and M. A. H. Ibrahim, "A new 4-D multi-stable hyperchaotic system with no balance point: Bifurcation analysis, circuit simulation, FPGA realization and image cryptosystem," *IEEE Access*, vol. 9, pp. 144555–144573, 2021.

[12] S. Vaidyanathan, A. Sambas, M. Mohamed, M. Mamat, W. Sanjaya, and Sudarno, "A new 2-D multi-stable chaotic attractor and its MultiSim electronic circuit design," *Indonesian J. Electr. Eng. Comput. Sci.*, vol. 22, no. 2, pp. 91–99, 2020.

[13] S. Vaidyanathan, I. M. Moroz, A. Sambas, M. A. Mohamed, M. D. Johansyah, M. Mamat, and M. Z. Ahmad, "A new multistable 4-D hyperchaotic four-scroll system, its dynamic analysis and circuit design," *Eng. Lett.*, vol. 29, no. 4, pp. 1311–1318, 2021.

[14] Z. Wang, R. Ramamoorthy, X. Xi, and H. Namazi, "Synchronization of the neurons coupled with sequential developing electrical and chemical synapses," *Math. Biosci. Eng.*, vol. 19, no. 2, pp. 1877–1890, 2021.

[15] Y. J. Monkam, S. T. Kingni, R. Tchitnga, and P. Woafo, "Electronic simulation and microcontroller real implementation of an autonomous chaotic and hyperchaotic system made of a Colpitts–Josephson junction like circuit," *Anal. Integr. Circuits Signal Process.*, vol. 110, no. 3, pp. 395–407, Mar. 2022.

[16] R. D. Méndez-Ramírez, A. Arellano-Delgado, M. A. Murillo-Escobar, and C. Cruz-Hernández, "A new 4D hyperchaotic system and its analog and digital implementation," *Electronics*, vol. 10, no. 15, p. 1793, Jul. 2021.

[17] M. A. Valencia-Ponce, P. R. Castañeda-Avińa, E. Tlelo-Cuautle, V. H. Carbajal-Gómez, V. R. González-Díaz, Y. Sandoval-Ibarra, and J.-C. Nuńez-Perez, "CMOS OTA-based filters for designing fractional-order chaotic oscillators," *Fractal Fractional*, vol. 5, no. 3, p. 122, 2021.

[18] N. Dahasert, I. Öztürk, and R. Kiliç, "Experimental realizations of the HR neuron model with programmable hardware and synchronization applications," *Nonlinear Dyn.*, vol. 70, no. 4, pp. 2343–2358, Dec. 2012.

[19] A. Silva-Juárez, E. Tlelo-Cuautle, L. G. de la Fraga, and R. Li, "FPAA-based implementation of fractional-order chaotic oscillators using first-order active filter blocks," *J. Adv. Res.*, vol. 25, pp. 77–85, Sep. 2020.

[20] H. A. Abdullah and H. N. Abdullah, "Design and FPGA implementation of novel chaotic system," *University Politechnica Bucharest Sci. Bull. Ser. C Electr. Eng. Comput. Sci.*, vol. 81, no. 2, pp. 153–164, 2019.

[21] F. Y. Dalkiran and J. C. Sprott, "Simple chaotic hyperjerk system," *Int. J. Bifurcation Chaos*, vol. 26, no. 11, Oct. 2016, Art. no. 1650189.

[22] N. Korkmaz and R. Kilic, "Implementations of modified chaotic neural models with analog reconfigurable hardware," *Int. J. Bifurcation Chaos*, vol. 24, no. 4, Apr. 2014, Art. no. 1450046.

[23] B. Abd-El-Atty, A. M. Iliyasu, A. El-Latif, and A. Ahmed, "A multi-image cryptosystem using quantum walks and Chebyshev map," *Complexity*, vol. 2021, pp. 1–16, Oct. 2021.

[24] A. A. A. El-Latif, A. M. Iliyasu, and B. Abd-El-Atty, "An efficient visually meaningful quantum walks-based encryption scheme for secure data transmission on IoT and smart applications," *Mathematics*, vol. 9, no. 23, p. 3131, Dec. 2021.

[25] A. Alanezi, B. Abd-El-Atty, H. Kolivand, A. El-Latif, A. Ahmed, A. El-Rahiem, S. Sankar, and H. S. Khalifa, "Securing digital images through simple permutation-substitution mechanism in cloud-based smart city environment," *Secur. Commun. Netw.*, vol. 2021, Feb. 2021, Art. no. 6615512.

[26] Z.-H. Gan, X.-L. Chai, D.-J. Han, and Y.-R. Chen, "A chaotic image encryption algorithm based on 3-D bit-plane permutation," *Neural Comput. Appl.*, vol. 31, no. 11, pp. 7111–7130, 2018.

[27] S. Zhou, X. Wang, Z. Wang, and C. Zhang, "A novel method based on the pseudo-orbits to calculate the largest Lyapunov exponent from chaotic equations," *Chaos: Interdiscipl. J. Nonlinear Sci.*, vol. 29, no. 3, Mar. 2019, Art. no. 033125.

[28] J. Yang, Z. Feng, and Z. Liu, "A new five-dimensional hyperchaotic system with six coexisting attractors," *Qualitative Theory Dyn. Syst.*, vol. 20, no. 1, p. 18, Mar. 2021.

[29] C. Xu, X. Wu, Y. He, and Y. Mo, "5D hyper-chaotic system with multiple types of equilibrium points," *J. Shanghai Jiaotong Univ. Sci.*, vol. 25, no. 5, pp. 639–649, 2020.

[30] H. Wang and X. Li, "A novel hyperchaotic system with infinitely many heteroclinic orbits coined," *Chaos, Solitons Fractals*, vol. 106, pp. 5–15, Jan. 2018.

[31] Y. Sui, Y. He, W. Yu, and Y. Li, "Design and circuit implementation of a five-dimensional hyperchaotic system with linear parameter," *Int. J. Circuit Theory Appl.*, vol. 46, no. 8, pp. 1503–1515, Aug. 2018.

[32] Z. Peng, W. Yu, J. Wang, Z. Zhou, J. Chen, and G. Zhong, "Secure communication based on microcontroller unit with a novel five-dimensional hyperchaotic system," *Arabian J. Sci. Eng.*, vol. 47, pp. 813–828, Mar. 2021.

[33] P. Trikha, L. S. Jahanzaib, and D. Baleanu, "Dynamical analysis and triple compound combination anti-synchronization of novel fractional chaotic system," *J. Vibrat. Control*, vol. 28, nos. 9–10, pp. 1057–1073, May 2022.

[34] S. Vaidyanathan, A. Sambas, B. Abd-El-Atty, A. A. A. El-Latif, E. Tlelo-Cuautle, O. Guillen-Fernandez, M. Mamat, M. A. Mohamed, M. Alcin, M. Tuna, I. Pehlivan, I. Koyuncu, and M. A. H. Ibrahim, "A 5-D multi-stable hyperchaotic two-disk dynamo system with no equilibrium point: Circuit design, FPGA realization and applications to TRNGs and image encryption," *IEEE Access*, vol. 9, pp. 81352–81369, 2021.

[35] Q. Yang and M. Bai, "A new 5D hyperchaotic system based on modified generalized Lorenz system," *Nonlinear Dyn.*, vol. 88, no. 1, pp. 189–221, Apr. 2017.

[36] F. Yu, L. Liu, B. He, Y. Huang, C. Shi, S. Cai, Y. Song, S. Du, and Q. Wan, "Analysis and FPGA realization of a novel 5D hyperchaotic four-wing memristive system, active control synchronization, and secure communication application," *Complexity*, vol. 2019, pp. 1–18, Nov. 2019.

[37] M. Aziz and S. Al-Azzawi, "Chaos control and synchronization of a novel 5-D hyperchaotic Lorenz system via nonlinear control," *Int. J. Modern Phys. Appl.*, vol. 2, pp. 110–115, Dec. 2015.

[38] Q. Lai, C. Lai, H. Zhang, and C. Li, "Hidden coexisting hyperchaos of new memristive neuron model and its application in image encryption," *Chaos, Solitons Fractals*, vol. 158, May 2022, Art. no. 112017.

[39] Q. Lai, C. Lai, P. D. K. Kuate, C. Li, and S. He, "Chaos in a simplest cyclic memristive neural network," *Int. J. Bifurcation Chaos*, vol. 32, no. 3, Mar. 2022, Art. no. 2250042.

[40] Q. Lai, Z. Wan, and P. D. K. Kuate, "Modelling and circuit realisation of a new no-equilibrium chaotic system with hidden attractor and coexisting attractors," *Electron. Lett.*, vol. 56, no. 20, pp. 1044–1046, Sep. 2020.
[41] M. A. Valencia-Ponce, E. Tlelo-Cuautle, and L. G. de la Fraga, "Estimating the highest time-step in numerical methods to enhance the optimization of chaotic oscillators," *Mathematics*, vol. 9, no. 16, p. 1938, Aug. 2021.
[42] Y.-Z. Cheng, F.-H. Min, Z. Rui, and L. Zhang, "Heterogeneous dual memristive circuit: Multistability, symmetry, and FPGA implementation," *Chin. Phys. B*, vol. 30, no. 12, Dec. 2021, Art. no. 120502.
[43] W. S. Sayed, M. Roshdy, L. A. Said, and A. G. Radwan, "Design and FPGA verification of custom-shaped chaotic attractors using rotation, offset boosting and amplitude control," *IEEE Trans. Circuits Syst. II, Exp. Briefs*, vol. 68, no. 11, pp. 3466–3470, Nov. 2021.
[44] F. Yu, H. Shen, Z. Zhang, Y. Huang, S. Cai, and S. Du, "A new multi-scroll Chua's circuit with composite hyperbolic tangent-cubic nonlinearity: Complex dynamics, hardware implementation and image encryption application," *Integration*, vol. 81, pp. 71–83, Nov. 2021.
[45] M. D. Gupta and R. K. Chauhan, "Secure image encryption scheme using 4D-hyperchaotic systems based reconfigurable pseudo-random number generator and S-Box," *Integration*, vol. 81, pp. 137–159, Nov. 2021.
[46] M. Gafsi, N. Abbassi, M. A. Hajjaji, J. Malek, and A. Mtibaa, "Xilinx Zynq FPGA for hardware implementation of a chaos-based cryptosystem for real-time image protection," *J. Circuits, Syst. Comput.*, vol. 30, no. 11, Sep. 2021, Art. no. 2150204.
[47] Z. Karaca, N. Korkmaz, Y. Altuncu, and R. Kılıç, "An extensive FPGA-based realization study about the Izhikevich neurons and their bio-inspired applications," *Nonlinear Dyn.*, vol. 105, no. 4, pp. 3529–3549, Sep. 2021.
[48] E. Tlelo-Cuautle, J. J. Rangel-Magdaleno, A. D. Pano-Azucena, P. J. Obeso-Rodelo, and J. C. Nunez-Perez, "FPGA realization of multi-scroll chaotic oscillators," *Commun. Nonlinear Sci. Numer. Simul.*, vol. 27, nos. 1–3, pp. 66–80, Oct. 2015.
[49] *Sipi Image Database misc*. Accessed: Jan. 10, 2022. [Online]. Available: https://sipi.usc.edu/database/database.php?volume=misc
[50] X. Wang and S. Gao, "Image encryption algorithm based on the matrix semi-tensor product with a compound secret key produced by a Boolean network," *Inf. Sci.*, vol. 539, pp. 195–214, Oct. 2020.

KHALED BENKOUIDER received the M.S. and Ph.D. degrees in automatic control from the University of Jijel, Jijel, Algeria, in 2015 and 2021, respectively. His M.S. research was on secure communications based on chaotic systems. His main research interests include dynamical systems, control systems, delayed systems, LPV systems, and chaotic systems synchronization.

SUNDARAPANDIAN VAIDYANATHAN received the D.Sc. degree in electrical and systems engineering from Washington University at St. Louis, St. Louis, MO, USA, in 1996. He is currently a Professor and the Dean of the Research and Development Centre, Vel Tech University, Chennai, India. He has published over 550 Scopus-indexed research publications. His current research interests include linear and nonlinear control systems, chaotic and hyperchaotic systems, circuits, intelligent control, optimal control, mathematical modeling, and scientific computing.

ACENG SAMBAS received the Ph.D. degree in mathematics from the Universiti Sultan Zainal Abidin (UniSZA), Malaysia, in 2021. He has been a Lecturer with the Muhammadiyah University of Tasikmalaya, Indonesia, since 2015. His current research interests include dynamical systems, chaotic signals, electrical engineering, computational science, signal processing, robotics, embedded systems, and artificial intelligence.

ESTEBAN TLELO-CUAUTLE received the B.Sc. degree from the Instituto Tecnológico de Puebla, Mexico, in 1993, and the M.Sc. and Ph.D. degrees from the Instituto Nacional de Astrofísica, Óptica y Electrónica (INAOE), Mexico, in 1995 and 2000, respectively. In 2001, he was appointed as a Professor-Researcher at the INAOE. He has authored five books, edited 11 books, and around 300 works published in book chapters, international journals, and conferences. His research interests include analog signal processing, synthesis and design of integrated circuits, optimization by metaheuristics, design and applications of chaotic systems, security in the Internet of Things, symbolic analysis, and analog/RF and mixed-signal design automation tools. He serves as an Associate Editor for the IEEE TRANSACTIONS ON CIRCUITS AND SYSTEMS—I: REGULAR PAPERS, *Engineering Applications of Artificial Intelligence*, *International Journal of Circuit Theory and Applications*, *Electronics*, *Integration, the VLSI Journal*, and *Frontiers of Information Technology and Electronics Engineering*.

AHMED A. ABD EL-LATIF (Senior Member, IEEE) received the B.Sc. degree (Hons.) in mathematics and computer science and the M.Sc. degree in computer science from Menoufia University, Egypt, in 2005 and 2010, respectively, and the Ph.D. degree in computer science and technology from the Harbin Institute of Technology, Harbin, China, in 2013. He is currently a Research Professor at the EIAS Data Science Laboratory, College of Computer and Information Sciences, Prince Sultan University, Riyadh, Saudi Arabia. He is the author or coauthor of more than 200 papers, including refereed IEEE/ACM/Springer/Elsevier journals, conference papers, books, and book chapters. He had many books, more than ten books, in several publishers for process in Springer, IET, CRC press, IGI-Global, Wiley, and IEEE. His research interests include multimedia content encryption, secure wireless communication, the IoT, applied cryptanalysis, perceptual cryptography, secret media sharing, information hiding, biometrics, forensic analysis in digital images, and quantum information processing. He is a fellow of the Academy of Scientific Research and Technology, Egypt. He received many awards, including the State Encouragement Award in Engineering Sciences in 2016, Arab Republic of Egypt; the Best Ph.D. Student Award from the Harbin Institute of Technology in 2013; and the Young Scientific Award, Menoufia University, Egypt, in 2014. He is an editor/guest editor in several reputed SCI journals.

BASSEM ABD-EL-ATTY received the B.S. degree in physics and computer science, the M.Sc. degree in computer science, and the Ph.D. degree in computer science from Menoufia University, Egypt, in 2010, 2017, and 2020, respectively. He is currently an Assistant Professor with the Faculty of Computers and Information, Luxor University, Egypt. He is the author or coauthor of more than 30 papers, including refereed articles published by IEEE, Elsevier, and Springer journals, conference papers, and book chapters. His research interests include quantum information processing and image processing. He is a reviewer in a set of reputable journals in Elsevier and Springer.

CIRO FABIAN BERMUDEZ-MARQUEZ received the B.Sc. degree from the Benemérita Universidad Autónoma de Puebla (BUAP), Mexico, in 2020. He is currently pursuing the M.Sc. degree in electronics with the Instituto Nacional de Astrofísica, Óptica y Electr onica (INAOE), Mexico. His research interests include chaotic systems, optimization by metaheuristics, embedded systems, and digital signal processing.

IBRAHIM MOHAMMED SULAIMAN received the Ph.D. degree in fuzzy systems from the Universiti Sultan Zainal Abidin (UniSZA), Malaysia, in 2018. Since 2021, he has been a Lecturer with the Universiti Utara Malaysia, Malaysia. He has published research articles in various international journals and attended international conferences. His research interests include numerical research, fuzzy nonlinear systems, and unconstrained optimization.

ALIYU MUHAMMED AWWAL received the B.Sc. degree from Gombe State University, the M.Sc. degree from Bayero University Kano, and the Ph.D. degree in applied mathematics from the King Mongkut's University of Technology Thonburi (KMUTT). He has authored or coauthored a number of research articles in high impact journals. His research interest includes iterative algorithms for solving nonlinear problems, such as numerical optimization problems, nonlinear least squares problems, and system of nonlinear equations with applications in signal recovery, image deblurring, and motion control.

POOM KUMAM (Member, IEEE) received the Ph.D. degree in mathematics from Naresuan University, Thailand. He is currently a Full Professor with the Department of Mathematics, King Mongkut's University of Technology Thonburi (KMUTT). He is also the Head of the Fixed Point Theory and Applications Research Group, KMUTT, and also with the Theoretical and Computational Science Center (TaCS-Center), KMUTT. He is also the Director of the Computational and Applied Science for Smart Innovation Cluster (CLASSIC Research Cluster), KMUTT. He has provided and developed many mathematical tools in his fields productively over the past years. He has over 800 scientific articles and projects either presented or published. He has editorial board journals more than 50 journals and also he delivers many invited talks on different international conferences every year all around the world. His research interests include fixed point theory, variational analysis, random operator theory, optimization theory, approximation theory, fractional differential equations, differential game, entropy and quantum operators, fuzzy soft set, mathematical modeling for fluid dynamics, inverse problems, dynamic games in economics, traffic network equilibria, bandwidth allocation problem, wireless sensor networks, image restoration, signal and image processing, game theory, and cryptology.